ISLAMIC UNIVERSITY OF TECHNOLOGY (IUT)

COMPUTATIONAL INVESTIGATION OF PULSATILE BLOOD FLOW IN THE MODELS OF ARTERIAL STENOSIS AND ANEURYSM

M.Sc. Engineering (Mechanical) THESIS

BY

MD. ABDUL KARIM MIAH
Department of Mechanical and Chemical Engineering
Islamic University of Technology (IUT), Gazipur-1704, Bangladesh.
STUDENT NO: 141603

SUPERVISED BY

DR. NURUL ABSAR CHOWDHURY

March 2018

COMPUTATIONAL INVESTIGATION OF PULSATILE BLOOD FLOW IN THE MODELS OF ARTERIAL STENOSIS AND ANEURYSM

BY

MD. ABDUL KARIM MIAH
STUDENT NO: 141603

A THESIS PRESENTED TO THE DEPARTMENT OF MECHANICAL AND CHEMICAL ENGINEERING, ISLAMIC UNIVERSITY OF TECHNOLOGY DHAKA IN PARTIAL FULFILMENT OF THE REQUIREMENT FOR THE AWARD OF DEGREE FOR

MASTER OF SCIENCE (M. Sc.) IN MECHANICAL ENGINEERING

March 2018

Candidate's Declaration

It is hereby declared that this thesis or any part of it has not been submitted elsewhere for the award of any degree or diploma.

Signature of the Candidate

_____

MD. ABDUL KARIM MIAH
Student No.: 141603
Session 2015-2016
Department of Mechanical and Chemical Engineering (MCE)
Islamic University of Technology (IUT), OIC
Board Bazar, Gazipur
Dhaka, Bangladesh.

Signature of the Supervisor

_____

Dr. Nurul Absar Chowdhury
Professor
Department of Mechanical & Chemical Engineering (MCE)
Islamic University of Technology (IUT), OIC
Board Bazar, Gazipur
Dhaka, Bangladesh.

Certificate of Approval

The thesis titled "Computational investigation of pulsatile blood flow in the models of arterial stenosis and aneurysm" submitted by Md. Abdul Karim Miah bearing Student No. 141603 of Academic Year 2015-2016 has been found as satisfactory and accepted as partial fulfillment of the requirement for the degree of Master of Science in Mechanical Engineering on 07 March, 2018.

BOARD OF EXAMINERS

---

1. **Dr. Nurul Absar Chowdhury**
   Professor
   Department of Mechanical and Chemical Engineering
   Islamic University of Technology (IUT)
   Board Bazar, Gazipur, Dhaka, Bangladesh.

Chairman (Supervisor)

---

2. **Dr. M. saiful Bari**
   Professor and Head
   Department of Cardiology
   Mymensingh Medical College

Co-Supervisor

---

3. **Dr. Md. Zahid Hossain**
   Professor and Head
   Department of Mechanical and Chemical Engineering
   Islamic University of Technology (IUT)
   Board Bazar, Gazipur, Dhaka, Bangladesh.

Ex-Officio

---

4. **Dr. Arafat Ahmed Bhuiyan**
   Assistant Professor
   Department of Mechanical and Chemical Engineering
   Islamic University of Technology (IUT)
   Board Bazar, Gazipur, Dhaka, Bangladesh.

Member

---

5. **Prof. Dr. Md. Arefin Kowser**
   Department of Mechanical Engineering
   Dhaka University of Engineering and Technology (DUET)
   Gazipur, Bangladesh.

Member (External)

Acknowledgements

I would like to begin by saying Alhamdullilah, expressing gratitde to Almighty Allah who made it possible for me to finish this project successfully on time. Equally saying a big thank to my supervisor Dr. Nurul Absar Chowdhury, Professor, Department of Mechanical and Chemical Engineering, IUT, for all his support, ideas about thesis, discussions, time and for explaining so patiently the hard topics and checking this thesis and, not to mention, for all his care and concern. These will ever remain in my memory. Thanks to my examiners for their constructive ideas, suggestions and double-checking my work.

I would also like to express my high gratitude to the Head of Department, Professor Dr. Zahid Hossain, for his continues encouragement and support during the period of my studies. Finally, I will like to express my lasting gratitude to my family members for their patience, support, encouragement, enthusiasm and prayers.

Table of Contents

List of Figures

List of Tables

Nomenclature

IEL	Internal Elastic Lamina
SMC	Smooth Muscle Cells
EEL	External Elastic Lamina
DES	Diethylstilbestrol
WHO	World Health Organization
AAA	Abdominal Aortic Aneurysm
Wo	Womersley Number
LES	Large-Eddy Simulation
LDA	Laser Doppler Anemometry.
Re	Reynolds Numbers
r.m.s.	Root Mean Square
St	Strouhal Number
FEM	Element Method
UVP	Ultrasonic Vibration Potential
PIV	Particle Image Velocimetry
FVM	Finite Volume Method
WSS	Wall Shear Stress

Abstract

A numerical analysis based on a finite volume approach is employed for a 2-D axisymmetric, incompressible, laminar flow of mean Reynolds number of 578 so as to simulate and compare the pulsatile blood flow in the models of arterial stenosis and aneurysm of the same sizes. Radial velocity distribution and Wall Shear Stress Distribution have been taken as the two key parameters for analyzing and comparing stenosis and aneurysm of the same sizes of 32% and 48% severity. These parameters have been compared using unsteady blood flow of two frequencies: Womersley number of 7.75 and 10. In addition, the extent of the effect of Womersley number has been discussed. A flow input waveform is presented in terms of sinusoid. The results implicate that the Womersley number has a little effect on the flow field when the sizes were varied, which indicates the dominance of viscous force on the flow field of the models considered. It has been observed that the size or the severity of the stenosis or aneurysm has great effect on the flow field and Wall Shear Stress effect is too high in the stenosis compared to that in aneurysm. It has been concluded too that, for a particular depth of stenosis and aneurysm, with the same flow inputs, WSS is too high in the stenosis compared to that in aneurysm indicating very high risk in stenosis.

1 Introduction

1.1 Human Heart

Human knowledge has been progressing since centuries but last few decades have been an explosion of knowledge in almost every aspect of life. In spite of such an advancement of knowledge, there are still few fields which are as new as it could have been to the stone-age people. One such field of study is the human body which is such a complex and fascinating system to study. There are many individual subsystems in human body which collectively work together as one organic entity. There are various important organs in the human body among which the heart can be argued to be the most important organ typically because of its function of circulating blood to all body parts. Typically human heart weighs about is 250-350 gm though diseased heart can have much higher weight. The dimension of an adult heart could be 12cm x8cm x6cm [1].

Heart is primarily comprised of 4 chambers namely left atrium, left ventricle, right atrium and right ventricle. The left side chambers handle the oxygenated blood whereas the right side chambers processed deoxygenated blood. The deoxygenated blood from right side of the heart flows to lungs, where it is loaded with oxygen and returns to the left side of the heart. The oxygenated blood from the left side of the heart flows to all tissues of the body (with the exception of the heart and lungs) [2]. Some of the facts of heart are truly mind boggling. For instance, it is estimated that the heart beats about 2.65 billion times and pumps about 194 million liters of blood in 70 years of life span. This is similar to an amount of blood contained in a swimming pool of dimension 1 km length, 100m width and 2m depth. Supply of blood to body

parts is such a crucial requirement for nourishment supplied through blood circulation to heart muscles for keeping itself in active state of pumping.[3]

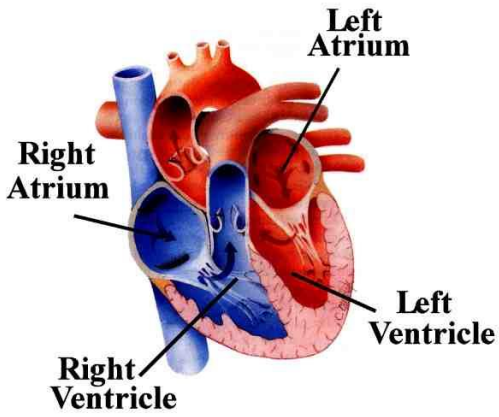

Figure 01: Human Heart [4]

1.2 Artery wall classification

Arteries transport oxygen rich blood around the body providing essential nutrients to vital organs. The artery wall consists of a complex multilayer porous substructure with an interstitial phase comprising predominantly of plasma. In a healthy artery this substructure is comprised of three concentric layers: the tunica intima, the tunica media and the tunica adventitia. The tunica intima is the innermost layer, consisting of a single layer of endothelial cells and a sub endothelial layer mainly consisting of delicate connective tissues and collagen fibers. The outer boundary of the tunica intima is surrounded by an elastic tissue with fenestral pores known as the internal elastic lamina (IEL). The medial layer consists primarily of concentric sheets of smooth muscle cells (SMC) within a loose connective tissue framework. This configuration of SMC

enables the artery wall to contract and relax. The tunica media and the tunica adventitia are separated by another thin band of elastic fibers known as the external elastic lamina (EEL). The outermost layer of the artery, the tunica adventitia, is comprised of connective tissue fibers and some capillaries. The fibers blend into the surrounding connective tissues and aid in stabilizing the arteries within the body. The target layer for the anti-restenotic drugs is the tunica media because SMC resides here and possible erosion of the tunica intima occurs upon stent deployment [5].

The artery wall is porous in composition and drug transport is facilitated through the surrounding plasma not only via diffusion but there is also the presence of a trans-mural velocity due to a pressure gradient observed across the artery wall. However, the presence of arterial plaque will reduce the magnitude of this trans-mural velocity and can even stem it altogether [6]. As DES is deployed in highly occluded arteries it is reasonable to reduce the complexity of the problem by neglecting convection on the wall. Arterial properties such as porosity, tortuosity and free diffusivity can influence the transport of drugs within the respective artery wall layers. The compression of these layers will alter these properties which in turn may inhibit the transport of species as governed by the mass transport equations. The compression of a porous structure not only reduces the materials porosity but it results in the creation of a more arduous pore path over which mass transport would normally occur. The combination of a reduced porosity with an increased tortuosity, when the artery wall has been compressed, has a net effect of reducing the effective diffusivity thus hindering mass transport within the vessel [5].

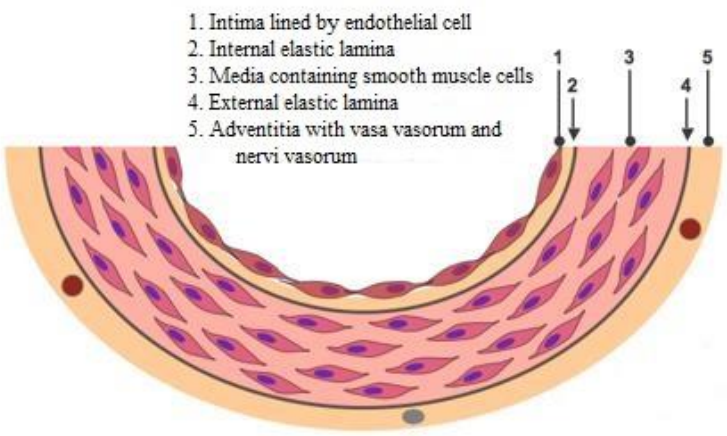

Figure 02: Cross sectional structure of a healthy arterial wall [7]

1.3 Background

The supply of blood to the heart muscles can get hindered leading to very serious diseases such as atherosclerosis. The atherosclerosis is characterized by thickening of arterial wall due to deposition of undesirable materials such as cholesterol, fatty substances, cellular waste products, calcium and fibrin (a clotting material in the blood) etc.

Heart disease is a disease in which a waxy substance called plaque builds up inside the arteries. These arteries supply oxygen-rich blood to your heart muscle.

When plaque builds up in the arteries, the condition is called atherosclerosis. The buildup of plaque occurs over many years. Over time, plaque can harden or rupture (break open). Hardened plaque narrows the arteries and reduces the flow of oxygen-rich blood to the heart [8].

If the plaque ruptures, a blood clot can form on its surface. A large blood clot can mostly or completely block blood flow through a artery. Over time, ruptured plaque also hardens and narrows the coronary arteries [9].

If the flow of oxygen-rich blood to your heart muscle is reduced or blocked, angina or a heart attack can occur.

Angina is chest pain or discomfort. It may feel like pressure or squeezing in your chest. The pain also can occur in your shoulders, arms, neck, jaw, or back. Angina pain may even feel like indigestion.

A heart attack occurs if the flow of oxygen-rich blood to a section of heart muscle is cut off. If blood flow isn’t restored quickly, the section of heart muscle begins to die. Without quick treatment, a heart attack can lead to serious health problems or death.

Over time, Heart disease can weaken the heart muscle and lead to heart failure and arrhythmias. Heart failure is a condition in which your heart can't pump enough blood to meet your body’s needs. Arrhythmias are problems with the rate or rhythm of the heartbeat [10].

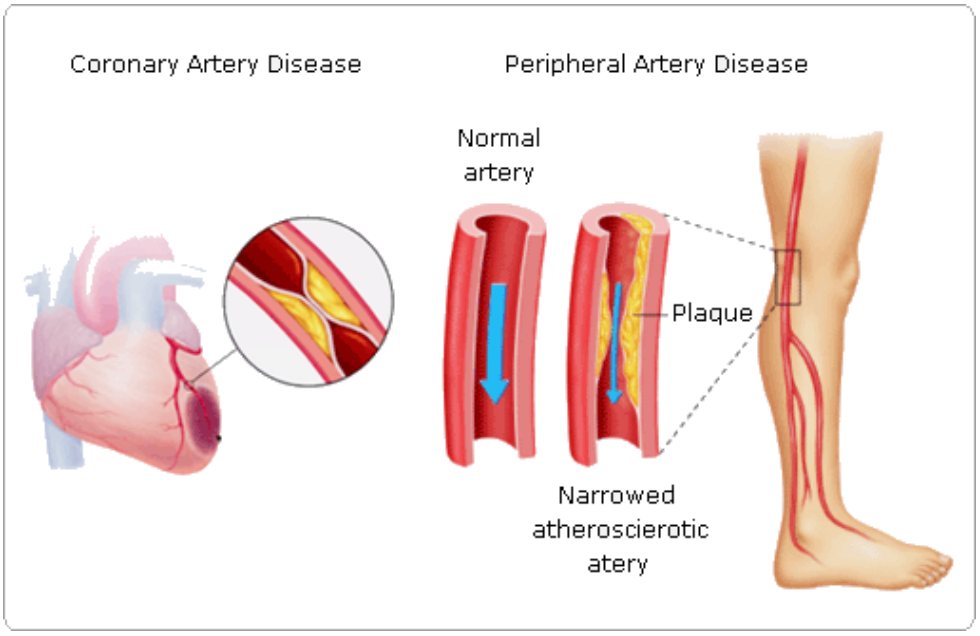

Figure 03: Stenosis in Coronary Artery and Peripheral Artery [11]

According to World Health Organization (WHO) fact sheet, coronary heart diseases is the most leading cause of death.

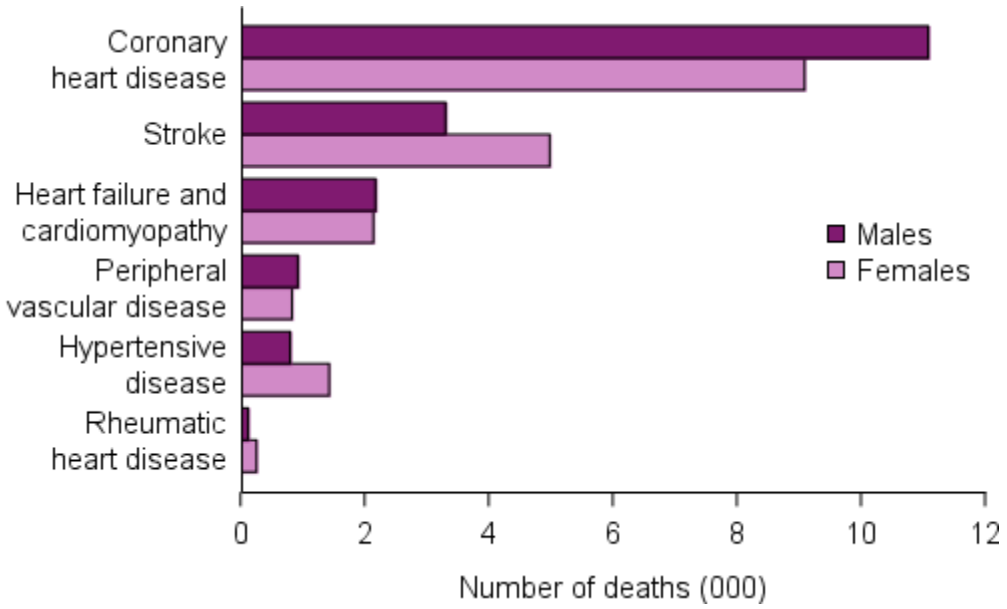

Figure 04: Leading causes of death [12]

An aneurysm is an abnormal swelling or bulge in the wall of a blood vessel, such as an artery. It begins as a weak spot in the blood vessel wall, which balloons out of shape over time by the force of the pumping blood. Usually, aneurysms develop at the point where a blood vessel branches, because the 'fork' is structurally more vulnerable. Aneurysms can occur anywhere throughout the circulatory system, but most commonly develop along the aorta (the body's main artery that runs the length of the trunk from the heart) and in blood vessels of the brain. Aneurysms are potentially fatal if they rupture. Death can occur within minutes [13].

A cerebral aneurysm occurs in a blood vessel in the brain. An aneurysm in the brain has no relationship to other aneurysms in the body, but in a small number of people, there is a family history. Cerebral aneurysms are more common over the age of 60.The aneurysm may appear like a tiny blood filled grape attached to the blood vessel by a stalk. This is known as a saccular or berry aneurysm. These can sometimes form in clusters. Symptoms of a ruptured cerebral

aneurysm include severe headache with rapid onset, neck pain and stiffness, increasing drowsiness, paralysis, seizures, impaired speech and visual problems. An unruptured cerebral aneurysm may have no symptoms related to it at all and may be discovered incidentally [13].

A thoracic aortic aneurysm affects the aorta in the chest. Symptoms of a ruptured thoracic aortic aneurysm include pain in the chest, back and neck, coughing, breathlessness, swallowing difficulties, hoarseness of the voice, swelling of the arms, and a constricted pupil and drooping of the eyelid affecting one eye. In many cases, a thoracic aortic aneurysm doesn't cause any symptoms and is discovered by accident during medical examinations for an unrelated condition [14].

An abdominal aortic aneurysm affects the aorta in the abdomen. Symptoms include pain in the lower back, abdominal swelling, nausea, vomiting, rapid heart rate (tachycardia), sweating and the sensation of a pulse in the abdomen.

The incidence of abdominal aortic aneurysm (AAA) is on the increase with approximately 150,000 new cases diagnosed in the US each year. Although the mortality rates associated with AAA are high, there still remains uncertainty about the correct time to surgically repair these aneurysms [15].

Abdominal aortic aneurysms (AAAs) are notoriously asymptomatic and often referred to as a ''silent killer''. Patients frequently present at hospital with abdominal and/or back pain, where examination reveals the cause of the pain to be a pulsating mass deep within the abdomen, in other words, an AAA.

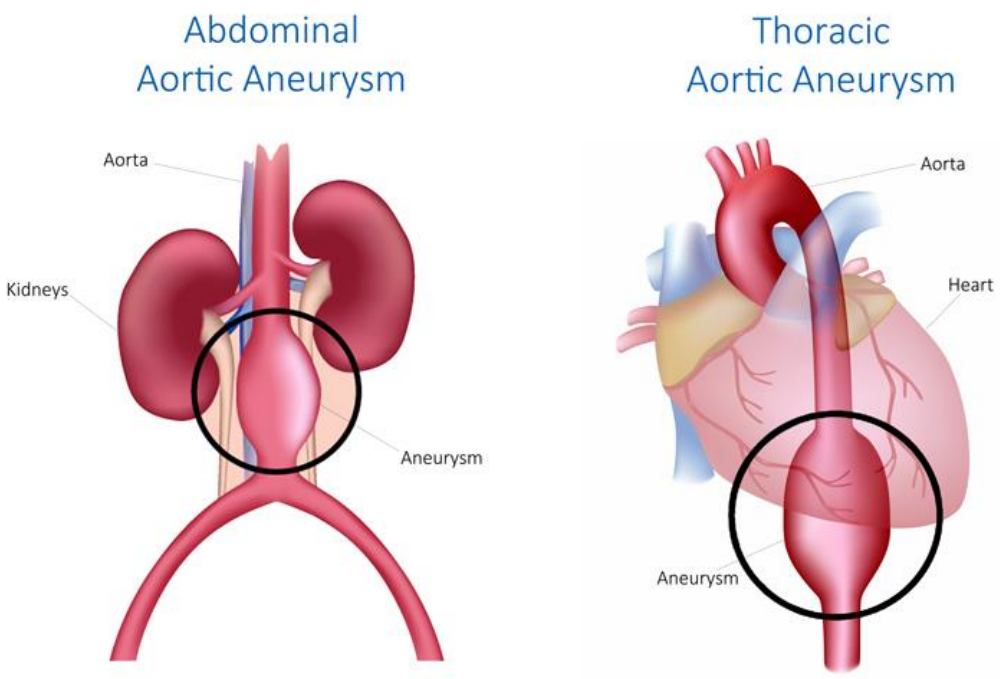

Figure 05: Aneurysm in Abdominal Aorta and Thoracic Aorta [16]

1.4 Literature Review

Blood flow through artery is very complex and investigation of its flow behavior is very important for its use in life science and medical technology. Since the hemodynamics hypotheses of atherosclerosis were first formulated several decades ago, flow imaging and computing have played an increasingly important role in advancing our understanding of how blood really flows in large arteries prone to atherosclerosis[17]. Many experimental and CFD analysis have been done to investigate the flow disorder due to formation of aneurism, two most widely spread disease, in human beings leading to the failure of cardiovascular system.

Arterial stenosis is an abnormal narrowing of one of the arteries, as defined by the National Institute of Neurological Disorders and Stroke. On the other hand an aneurism is an excessive

localized enlargement of an artery caused by weakness in the artery wall. The presence of a stenosis or an aneurysm in an artery may significantly alter the flow field and consequently the flow rate, leading to severe pathological incidences. Stenosis increases the risk for stroke because it reduces blood flow. The heart then needs to squeeze (contract) harder to pump blood. Whereas the development of an aneurysm and its continuous dilation may lead to its rupture causing death or grave disability.

The main goal of blood flow simulation in vessels is to evaluate hemodynamic forces which artery wall experiences due to different factors like the pulsatile blood flow, the fluid flow geometry and the blood rheology behavior (quasi-Newtonian or non-Newtonian fluid). Besides, it is important to know if there is any observable correlation between flow pattern characteristics and abnormal biological events and arterial diseases.

It is proved that hemodynamic parameters play fundamental roles in the regulation of vascular biology and access of arterial diseases[18]. Wall shear stress, particle residence time, recirculation zones and arterial wall strain are examples of hemodynamic parameters. Formations of dysfunctions in vascular biology are results of irregular variation of these parameters.

Several numerical and experimental works have been done to observe the blood flow behaviors using aneurysm and stenosis models considering the flow as pulsatile.

Ojha et al.[19] investigated flow behavior through arterial stenosis experimentally using the photochromic tracer method to record pulsatile flow velocity profile. He observed the velocity profile at three axial locations along a flow channel. Flow patterns in tubes with mild to moderate degrees of vessel constriction were performed. 2.9 Hz sinusoidal flow superimposed on a steady flow was used. Isolated regions of vortical and helical structures were observed

primarily during the deceleration phase of the flow cycle and in the vicinity of the reattachment point in the mild constrictions. These effects were more visible for asymmetric condition. Transition to turbulence was triggered just before peak flow through the breakdown of waves and stream-wise vortices that were shed in the high-shear layer for the moderate constriction.

Mittal et al.[20] studied pulsatile blood flow through modeled arterial stenosis using the consisting of technique of large-eddy simulation (LES). One-sided 50% semicircular constriction in a planner channel for the study. A peak Reynolds number of 2000 and a Strouhal number of 0.024 were taken. It was observed that the flow downstream of the stenosis transitions to turbulence and exhibits all the classic features of post-stenotic flow and it includes the periodic shedding of shear layer vortices and transition to turbulence downstream of the stenosis.

Modarres, Seyedein and Shahabi [21] computed Hemodynamic wall parameters at three Womersley numbers and compared them for three rheology models (Newtonian, Power law and Quemada) in the tubular flow with a smooth local occlusion. Results show that Quemada model always located between Newtonian and Power law models however its behavior is closer to Power law model. Concerning this behavior and better agreement between Quemada and experimental blood viscosity, it can be expected that Quemada results are more realistic and accurate.

Toufique and Dipak [22] investigated the effect of pulsation, stenosis size, Reynolds Number and Womersley number using the laminar flow through a model arterial stenosis with a trapezoidal profile. They used up to peak Reynolds number of 1000. Generation of recirculation zone was observed in the post stenosis zone on account of the dynamic nature of the pulsating

flow disturbance in the radial velocity distribution. The peak wall shear stress develops for 65% stenosis (by area) is 3, 2.2, and 1.3 times higher than that for 30%, 45%, and 55% stenosis, respectively. It is also observed that the peak wall vorticity seems to increase with the increase of stenosis size and Reynolds number.

Ali et al. [23] studied unsteady pulsatile flow of blood through a tapered stenotic artery in which the Sisko model was used. A realistic geometry of the time-variant stenosis is considered for the present analysis. The problem is modeled under the assumption that the lumen radius is sufficiently smaller than the wavelength of the pulsatile pressure wave. Employing the finite difference method, the governing equations are integrated along with the prescribed boundary conditions over the whole arterial segment under consideration. The radial and axial velocity, volumetric flow rate, resistance impedance and wall shear stress are analyzed for various values of the emerging parameters through graphical results.

W. Y. Chan, Y. Ding and J. Y. Tu [24] investigated fluid and structural responses to pulsatile non-Newtonian blood flow through a stenosed artery, using ANSYS. The artery was modeled as an axisymmetric stenosed vessel. Isotropic and elastic wall was used. The blood behavior was described by the Power Law and the Carreau non-Newtonian models, respectively. When compared to the Newtonian flow models, the result from the Carreau model showed very little difference, in terms velocity, pressure and wall shear stress, whereas the result from the Power Law model showed more significant vortices and smaller wall shear stresses. The highest stress concentration was also found at the throat of the stenosis.

Ahmed and Giddens[25] investigated the pulsatile flow field using axisymmetric constrictions in a straight tube using laser Doppler anemometry. They used a sinusoidal velocity waveform with a frequency of 7.5 and mean Reynolds number 600. Stenosis with different severities were employed. The experiments indicate that a temporary region of post-stenotic flow separation exists even for most severe constriction. Wall shear stresses were found to be maximum near the constriction and relatively low in the post-stenotic region. The present study implies that identification of flow disturbances of an organized nature may be fundamental in recognizing mild to moderate disease.

Ali, Zaman and Sajid [23] presented a mathematical study for unsteady pulsatile flow of blood through a tapered stenotic artery. Constitutive Sisko model has been used to observe the rheology of blood. A realistic geometry of the stenosis is considered in the analysis. Lumen radius was taken sufficiently smaller than the wavelength of the pulsatile pressure wave. Employing the finite difference method, the governing equations are integrated along with the prescribed boundary conditions over the whole arterial segment. Various flow parameters like radial and axial velocity, volumetric flow rate, resistance impedance and wall shear stress were analyzed.

Berger and Jou [17] reviewed the modeling studies and experiments on steady and unsteady, two-and three-dimensional flows in arteries and geometries relevant to atherosclerosis.These include studies of normal vessels-to identify, on the basis of the fluid mechanics, lesion foci-and stenotic vessels, to model and measure flow in vessels after the lesions have evolved into plaques sufficiently large to significantly modify the flow.

Deshpande et al. [26] presented numerical solutions for steady flow through axisymmetric, contoured constrictions in a rigid tube, utilizing the full Navier-Stokes equations in cylindrical coordinates. No difficulties in convergence are encountered for Reynolds numbers at which the flow is known to be laminar from experimental observation. The theoretical results are compared with available experimental data, and the relationships to occlusive vascular disease are discussed.

Huang et al.[27] investigated flow in a tube with an occlusion. They used a finite difference scheme. The results are interpreted in the context of blood flow in stenosed arteries. Numerical results for steady and pulsatile flows confirm that a high shear stress is not likely to initiate atherosclerosis lesions. The study of unsteady flow reveals several interesting new features. It appears that there is a correlation between regions of recirculation, which are a prominent feature of the unsteady flow. Experimental measurements for steady flow complement the numerical study and show qualitative agreement.

Ishikawa et al.[28] numerically analyzed periodic blood flow through a stenosed tube. The bi-viscosity model is used as a constitutive equation for blood, and the flow is assumed to be periodic, incompressible and axisymmetric. Effects of pulsation and the rheological property of blood are considered. The flow pattern, separated region and the distributions of pressure and shear stress at the wall are obtained. The results show that the non-Newtonian property reduces the strength of the vortex downstream of stenosis and has considerable influence on the flow even at high Stokes and Reynolds numbers, provided that pulsatile flow has a stagnant period.

Lee[29] studied numerically the flow fields in around the double constrictions in a circular cylindrical tube. The effects on different flow parameters as the flow passes through the constrictions in the tube were studied. And the range of Reynolds number were chosen to be 5-200. It is noted that when the Reynolds number is below 10, no recirculation region is formed in the above constricted flow. For Reynolds numbers greater than 10, a recirculation region forms downstream of each of the constrictions. For constriction spacing ratios of 1,2, and 3, when the Reynolds number is high, a recirculation region spreads between the valley of the constrictions. When the Reynolds number is increased, the peak wall vorticity value increases and its location is moved upstream. Maximum wall vorticity generated by the first constriction is found to be always greater than the maximum wall vorticity generated by the second constriction.

Liao et al.[30] presented a thorough analysis on the characteristics of transitional turbulent flow over a bell-shape stenosis for a pulsatile flow. The comparison of the numerical solutions to different types of pulsatile flows was made. Then the effects of the Reynolds number, Womersley number and constriction ratio of stenosis on the pulsatile turbulent flow fields for the physiological flow are considered. The comparison of the different pulsatile flows shows that the flow characteristics cannot be properly estimated if an equivalent or simple pulsatile in flow is used instead of actual physiological one in the study of the pulsatile flows. For a physiological flow, the recirculation zones with high disturbance intensity occur mainly in the distal of the stenosis. The larger Reynolds number and severer constriction ratio may result in more complex flow field.

Mahapatra et al.[31] numerically solved unsteady Navier-Stokes equations by finite-difference technique. They considered staggered grid distribution for a flow through a channel with locally

symmetric and asymmetric constrictions. The critical Reynolds number for asymmetric flow through a symmetric constriction has been found. Critical values depend on the area reduction and the length of the constriction. An increase of Reynolds number grows the asymmetry of the flow. The root mean square (r.m.s.) centerline vertical velocity for asymmetric flow through a symmetric constriction has been drawn at different Reynolds numbers. For flow through symmetric constriction the centerline vertical velocity exhibits finite oscillation behind the constriction at high Reynolds number.

Neofytou and Tsangaris [32] numerically investigated the effects of different blood rheological models with the use of two 3D models of stenosis and an abdominal aortic aneurysm model. The employed CFD code incorporates the SIMPLE scheme in conjunction with the finite volume method. Three non-Newtonian models are employed, namely the Casson, Power-Law and Quemada models to observe the rheological behavior of blood. A comparison is made between the effects of each rheological models. Results show marked differences between simulating blood as Newtonian and non-Newtonian fluid and furthermore the Power-Law model exhibits different behaviour in all cases compared to the other models.

Tu and Deville[33] solved the problem of blood flow through stenosis using the incompressible generalized Newtonian model. They applied the Herschel-Bulkley, Bingham and power-law of fluids. The geometry taken was a rigid circular tube with a partial occlusion. Calculations are performed by a finite-element method. Results are obtained for steady and pulsatile physiological flows. Computations show that the memory effects taken into account in the model affect deeply the flow compared with the Newtonian reference case.

Zendehbudi and Moayeri [34] presented numerical solutions for a physiological pulsatile flow as well as for an equivalent simple pulsatile flow, having the same stroke and the differences in their flow behavior are discussed. The analysis is restricted to laminar flow, Newtonian fluid and axisymmetric rigid stenosis. Comparison of results shows that the behaviors of the two flows are similar at some instances of time, however, important observed differences indicate that for thorough understanding of pulsatile flow behavior in stenosed arteries, the actual physiological flow should be simulated.

Kumar et al.[35] numerically analyzed nonlinear axisymmetric pulsatile blood flow dynamics in rigid vessels with varying degrees of dilation using a transient UVP finite element method (FEM). The central axis velocity, central axis and wall pressures, pressure gradient history, and wall shear stress were found to be influenced by the presence of aneurysm. Time-dependent recirculation regions which are sensitive to the degree of dilation of the vessel are seen in the concavity of the dilation. The transverse velocities and their variations with time are found to be significant. High shear stresses were noticed near the ends of aneurysm that can lead to the development of stenosis in the region downstream from the dilation of the vessel.

Husain et al.[36] investigated the pulsatile simulations of blood flow through two three-dimensional models of an arterial stenosis and an aneurysm. Four non-Newtonian blood models, namely the Power Law, Casson, Carreau and the Generalized Power Law, as well as the Newtonian model of blood viscosity, are used to investigate the flow effects induced by these different blood constitutive equations. The aim of this study were three fold: firstly, to

investigate the variation in wall shear stress in an artery with a stenosis or aneurysm at different flow rates and degrees of severity; secondly, to compare the various blood models and hence quantify the differences between the models and judge their significance and lastly, to determine whether the use of the Newtonian blood model was appropriate over a wide range of shear rates.

Gopalakrishnan et al.[37] carried out numerical computations of pulsatile flows through aneurysm models and a stability analysis of these flows. The volume flow rate waveforms into the aneurysms were based on measurements of these waveforms, under rest and exercise conditions, of patients who were suffering from abdominal aortic aneurysms. The Reynolds number and Womersley number, the dimensionless quantities that characterize the flow, were varied within the physiologically relevant range, and the two geometric quantities that characterize the model aneurysm were varied to assess the influence of the length and maximal diameter of an aneurysm on the details of the flow. The results suggest that long aneurysms are less pathological than short ones, and that patients with an abdominal aortic aneurysm are better to avoid physical exercise. The abdominal aortic aneurysm can be viewed as acting like a 'wavemaker' that induces disturbed flow conditions in healthy segments of the arterial system far downstream of the aneurysm. Finally, they reported a remarkable sensitivity of the wall shear stress distribution and the growth rate of three-dimensional disturbances to small details of the aneurysm geometry near the proximal end.

Finol et al.[38] examined the hemodynamics of pulsatile blood flow in hypothetical three-dimensional models of abdominal aortic aneurysms (AAAs). Numerical predictions of blood flow patterns and hemodynamic stresses in AAAs are performed in single-aneurysm, asymmetric, rigid wall models. Finite element method was used. They characterized pulsatile

flow dynamics in AAAs for average resting conditions by means of identifying regions of disturbed flow and quantifying the disturbance. Physiologically realistic abdominal aortic blood flow was simulated under pulsatile conditions. Peak wall shear stress and peak wall pressure are reported as a function of the time-average Reynolds number and aneurysm asymmetry. The effect of asymmetry in hypothetically shaped AAAs is to increase the maximum wall shear stress at peak flow and to induce the appearance of secondary flows in late diastole.

Considerable amount of works have been done to observe the variation of different parameters in the blood flow in different modeled stenosis and also aneurysm. Stenosis and aneurysm of different shapes and sizes were studied. However, to the best of author's knowledge, no studies have been attempted to compare the flow behavior for the same sized stenosis and aneurysm. In this numerical modeling, the blood flow behavior using the stenosis and aneurysm of the same size has been studied to investigate the effects of laminar sinusoidal flow through the modeled artery.

1.5 Aims and Objectives

- ✓ To measure the variation of flow parameters (e.g. velocity distribution) in the stenosis and aneurysm as the effect is severe at this region.
- ✓ To find the variation of wall shear stresses with time in both the models and to find the region of maximum shear in the models as well.
- ✓ To compare the key parameters of the flow for different depths of stenosis and aneurysm

- ✓ To investigate the disorder of the flow between the stenosis and aneurysm of the same depth and same flow condition applied
- ✓ To find the effect of flow frequencies on the flow parameters.

1.6 Scope of Study

In this thesis work, a numerical simulation has been carried out to investigate the effects of laminar sinusoidal flow through the modeled arterial stenosis and aneurysm and the results were compared to observe which of the two are more dangerous for the patients with the same parameters. Here models of the stenosis and aneurysm have been chosen with the same severity. For both the models, the trapezoidal profile with an angle of 45^0 has been used to observe the effects on them. The models were axisymmetric. Sizes were varied from 32% severity to 48% severity with the corresponding depth of 1.6mm and 2.4mm respectively. Inlet flow given was the sinusoidal pulsating with a mean Reynolds Number of 578 having maximum of 928 and a minimum value of 228.Womersley numbers of 7.75 and 10 with a time periods of 345 milliseconds and 200 milliseconds respectively were used to see the effect of the change of the flow pulsation. Radial velocity distribution and Wall Shear Stress distribution have been chosen as the key parameters to observe the effects of change of Womersley number and sizes of the stenosis and aneurysm. .

2 Research Methodology

2.1 Numerical method of fluid flow

Numerical study has become an essential part of any research activity covering a wide range of human knowledge. This is particularly true for the case of scientific studies that are plagued by too much complexity in geometry involved or the difficult boundary conditions of complex problems. Hemodynamic is one such field that has been immensely benefitted by employing the techniques originating from numerical mathematics. Numerical Study is extensively used in biomechanics in recent years to have a better understanding of blood flow in the human body due to the intricacy involved in the vessel geometry as well as the complex hemodynamic mechanism. Among the numerical techniques, finite volume is the most popular technique for hemodynamic study. These techniques deal with the governing Navier Stokes equations which are too difficult to solve, thus most of the numerical studies being carried out revolve around the sophisticated software that has helped immensely in tackling such complex phenomenon. These techniques essentially require that the actual domain be divided into a number of smaller segments generally known as elements. The governing equations are applied to these small segment of the whole domain and the continuous solution is obtained over entire set of elements that provide continuity at the nodal points. These numerical techniques are well coded into a number of software tools. A technique based on fluid dynamic analysis namely Computational Fluid Dynamics (CFD) is gaining popularity in assessing the flow dynamics of blood inside the arteries which is proving to be a useful tool in clinical decision making. Among the available solvers in ANSYS, ANSYS Fluent is well-known and widely used.

2.2 Computational Fluid Dynamics

Computational fluid dynamics or CFD is the analysis of the system involving fluid now, heat transfer and associated phenomenon such as chemical reactions by means of computer-based simulation. The technique is very powerful and spans a Wide range of industrial and non-industrial application areas. It has emerged as one of the most powerful numerical tools for engineers, scientists and mathematicians alike. Its foundations are based on theoretical analysis drawn from experimental observations over various branches of physics.

There are several unique advantages of CFD over the experiment based approaches to the fluid system design. Some of those are:

- ✓ Substantial reduction of lead time and cost of new designs
- ✓ Ability to study system where controlled experiments are difficult or impossible to perform
- ✓ Ability to study systems under hazardous conditions at and beyond their normal performance limit
- ✓ Practically unlimited level of detail of results

The starting point for any computational analysis is the appropriate allocation of the governing equations. These equations are then substituted with equivalent numerical descriptions that are then solved using appropriate mathematical techniques. There are a number of numerical techniques available that will return a solution to a specified problem. Three of the more popular methods are the finite volume method, the finite element method and finite difference method. Three mathematical concepts are useful to determine the success of such methods: convergence, consistency and stability.

Convergence is the property of a numerical method to produce a solution which approaches the exact solution as the grid spacing; control volume size is reduced to zero. Consistent numerical schemes produce system of algebraic equations which can be demonstrated to be equivalent to the original governing equations the grid spacing tends to zero. Stability is associated with damping of errors as the numerical method proceeds. If a technique is not stable even round-off errors in the initial data can cause wild oscillations or divergence.

From the numerical methods mentioned above, finite volume method was selected as

- ✓ It uses integral form of conservation equations applied to each control volume: conservative laws are properly satisfied
- ✓ It is simplest to understand and easy to program
- ✓ Solution found from this method has more physical significance as the method flexible to system geometry and physical properly of fluid
- ✓ Finite volume method has more application in fluid mechanics field

The other two numerical methods can be summarized as follows

Finite difference method:

- ✓ Uses differential form and directly applied to grid points.
- ✓ Conservative laws are not properly satisfied

Finite element method:

- ✓ Used for unstructured grid which makes numerical solution to be complicated
- ✓ More popular in solid mechanics

For the above mentioned reasons finite volume method is selected for simulation.

2.2.1 Finite volume method

Finite volume method was originally developed as a special finite difference formulation. It is one of the most well-established and thoroughly validated general purpose CFD techniques. It is the central to four of the five main commercially available CFD codes: PHOENICS, FLUENT, FLOW3D and STAR-CD. This method consists of the following steps:

- ✓ Formal integration of the governing equations of the fluid flow over all the control volumes of the solution domain
- ✓ Discretization involves the substitution of a variety of finite difference type approximations for the terms in the integrated equation representing flow processes such as convection, diffusion and sources. This converts the integral equations into a system of algebraic equations
- ✓ Solution of the algebraic equations by an iterative methods

The first step, the control volume integration, distinguishes the finite volume method from all other CFD techniques. The resulting statements express the conservation of relevant properties for each finite size cells. This clear relationship between the numerical algorithm and the underlying physical conservation principle forms one of the main attractions of the finite volume methods and make its concepts much simpler to understand. For a certain variable Ø, the general conservation equation of the finite volume method is:

$$\begin{bmatrix} Rate\ of\ change \\ of\ \emptyset \text{ in control} \\ \text{volume with} \\ \text{respcet to time} \end{bmatrix} = \begin{bmatrix} Net\ flux\ of \\ \emptyset \text{ due to} \\ \text{convection into} \\ control\ volume \end{bmatrix} + \begin{bmatrix} Net\ flux\ of \\ \emptyset \text{ due to} \\ \text{diffusion into} \\ control\ volume \end{bmatrix} + \begin{bmatrix} Net\ rate\ of \\ creation\ of\ \emptyset \\ \text{inside the control} \\ volume \end{bmatrix}$$

CFD codes for finite volume technique contains discretization techniques suitable for the treatment of the key transport phenomenon, convection and diffusion as well as source terms and the rate of change with respect to time. The underlying physical phenomenon is complex a non-linear so an iterative solution approach is required.

Finite approach guarantees local conservation of a fluid property Ø for each control volume. Numerical schemes which possess the conservativeness property also ensure global conservation of the fluid property for the entire domain. This is clearly important physically and is achieved by means of consistent expressions for fluxes of Ø through the cell faces of the volumes.

2.2.2 Computational procedure of ANSYS Fluent

Our numerical simulation/calculation is done based on the Finite Volume Method (FVM) in ANSYS Fluent. Pressure based solver is used. In the Pressure-based methods the velocity is obtained from the momentum equations. The pressure field is extracted by solving a pressure or pressure correction equation, which is derived by manipulating continuity and momentum equations. In this solver, pressure-velocity coupling process is used in which equations of pressure are derived from the continuity and momentum equations. Pressure based coupled algorithm is chosen so that equations for all variables are solved for a given control volume at the same time.

Second order upwind scheme in spatial discretization is used where quantities at cell faces are computed, with high accuracy, through a Taylor series expansion of the cell centered solution about the cell centroid.

The solution domain is subdivided into a finite number of small control volumes (cells) by a grid. In the finite-volume approach, the integral form of the conservation equations are applied to the control volume defined by a cell to get the discrete equations for the cell. The cells are of quadrilateral shape (structured mesh). The grid defines the boundaries of the control volumes while the computational node lies at the center of the control volume. The domain is divided, by ANSYS Meshing Software, into small cells in such a way that the cell size is smaller, occupying higher number of cells, near the stenosis/Aneurysm and also on the post stenotic region where higher gradient of variables are naturally expected.

Time step size in the transient flow simulation is set by the error estimation of all variables between each successive time steps. Limiting convergence criteria for the solution is set to 1e-6 for all equations.

2.3 Mathematical Modelling/Governing Equations

General continuity and Navier-Stokes equation for the fluid flow is reduced for axisymmetric flow of incompressible, Newtonian fluids. The general continuity equation for fluid flow-

$$\frac{\partial \rho}{\partial t} + \Delta.(\rho \boldsymbol{u}) = 0$$

Which for incompressible flow in two dimensional cylindrical co-ordinate (r, X) can be reduced to-

$$\frac{1}{r}\frac{\partial(r\boldsymbol{u}_r)}{\partial x}+\frac{\partial(\boldsymbol{u}_x)}{\partial x}=0$$

General form of Navier-Stokes equation (with no body force) in the vector form is-

$$\rho\frac{\partial \boldsymbol{u}}{\partial t}+\ \rho\boldsymbol{u}.\nabla\boldsymbol{u}=-\nabla\mathrm{p}+\nabla^2\boldsymbol{u}$$

Which for incompressible flow in two dimensional cylindrical co-ordinate (r, X) can be reduced to the following.

Momentum in r direction:

$$\frac{\partial \boldsymbol{u}_r}{\partial t}+\boldsymbol{u}_r\frac{\partial \boldsymbol{u}_r}{\partial r}+\boldsymbol{u}_x\frac{\partial \boldsymbol{u}_r}{\partial x}=-\frac{1}{\rho}\frac{\partial p}{\partial r}+\frac{\mu}{\rho}[\frac{\partial}{\partial r}(\frac{1}{r}\frac{\partial(r\boldsymbol{u}_r)}{\partial r}+\frac{\partial^2\boldsymbol{u}_r}{\partial x^2})$$

Momentum in X-direction:

$$\frac{\partial \boldsymbol{u}_x}{\partial t}+\boldsymbol{u}_r\frac{\partial \boldsymbol{u}_x}{\partial r}+\boldsymbol{u}_x\frac{\partial \boldsymbol{u}_x}{\partial x}=-\frac{1}{\rho}\frac{\partial p}{\partial x}+\frac{\mu}{\rho}[\frac{1}{r}\frac{\partial}{\partial r}\left(r\frac{\partial(\boldsymbol{u}_x)}{\partial r}+\frac{\partial^2\boldsymbol{u}_x}{\partial x^2}\right)$$

Here, r = radial co-ordinate

x = axial co-ordinate locating at the axis of the symmetrical tube

$\mathbf{u}_r$ = total velocity in radial direction

$\mathbf{u}_x$ = total velocity in axial direction

p=pressure

ρ = density

μ = dynamic viscosity

2.4 2-Dimensional Computational models of Artery and Stenosis

2.4.1 Stenosis Model

ANSYS Design Modeler has been used for the generation of the stenosis and aneurysm models.

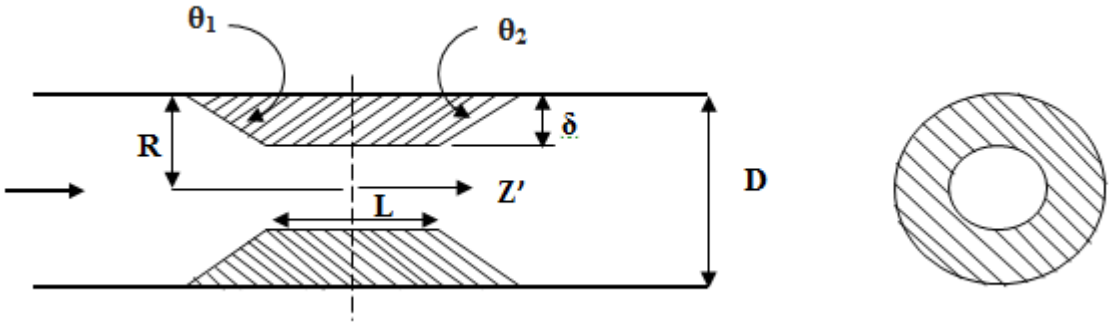

Figure 06: Geometry of the stenosis and Aneurysm used in the simulations, where L=length at the end portion, D=diameter of the unaffected tube, $\boldsymbol{\delta}$ = depth of stenosis, Z'=Z/D (normalized distance from the center of the stenosis. on the right side is the cross sectional view of models)

Stenosis severity has been defined as:

$$\frac{depth\ of\ the\ stenosis}{unaffected\ tube\ diameter}$$

For the present numerical simulation in figure **06**, $\theta_1=45^0$ and $\theta_2=45^0$ have been considered.

2.4.2 Aneurysm Model

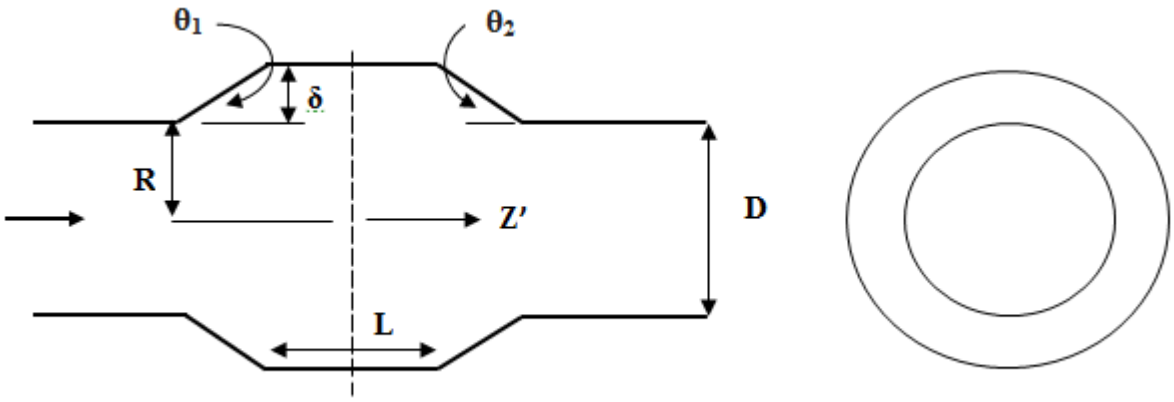

Figure 07: Geometry of the Aneurysm used in the simulations, where L=length at the end portion, D=diameter of the unaffected tube, $\boldsymbol{\delta}$ = depth of aneurysm, Z'=Z/D (normalized distance from the center of the stenosis. on the right side is the cross sectional view of models**)**

Aneurysm severity has been defined as:

$$\frac{depth\ of\ the\ aneurysm}{unaffected\ tube\ diameter}$$

For the present numerical simulation in figure **07,** $\theta_1=45^0$ and $\theta_2=45^0$ have been considered.

2.4.3 Grid Independence Test of Stenosis and Aneurysm

Numerical result should be independent of the inlet and outlet lengths of the artery from the stenosis/aneurysm. To find the independent inlet and outlet lengths from the stenosis/aneurysm, several simulation were carried out. Finally, it was seen that 20D and 60D lengths were sufficient for the proximal and distal side of the aneurysm/stenosis respectively. Moreover, mesh is a vital factor for the accuracy of the simulated result. To ensure the accuracy of the simulated results, several simulations were carried out with different mesh/gird shapes, several calculations were done with different number of elements. Finally, the chosen shape was the quadrilateral in 2D space as shown in figure 08 and figure 09, and different optimized elements for different stenosis grids and aneurysm grids were chosen: 50592 for 32% stenosis, 50597 for 48% stenosis, 51648 for 32% aneurysm, and 52400 for 48% aneurysm.

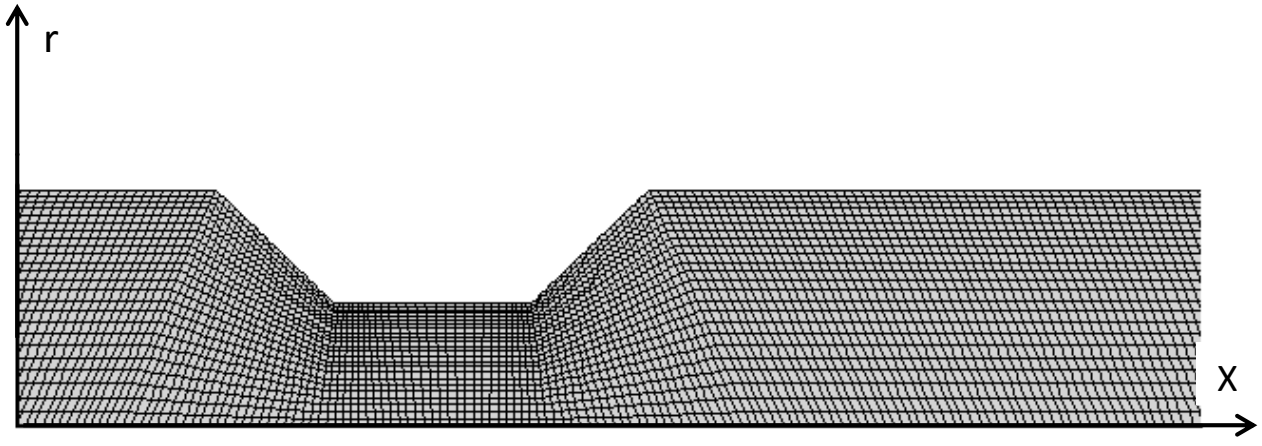

Figure 08: Discretization of the computational domain (for Stenosis)

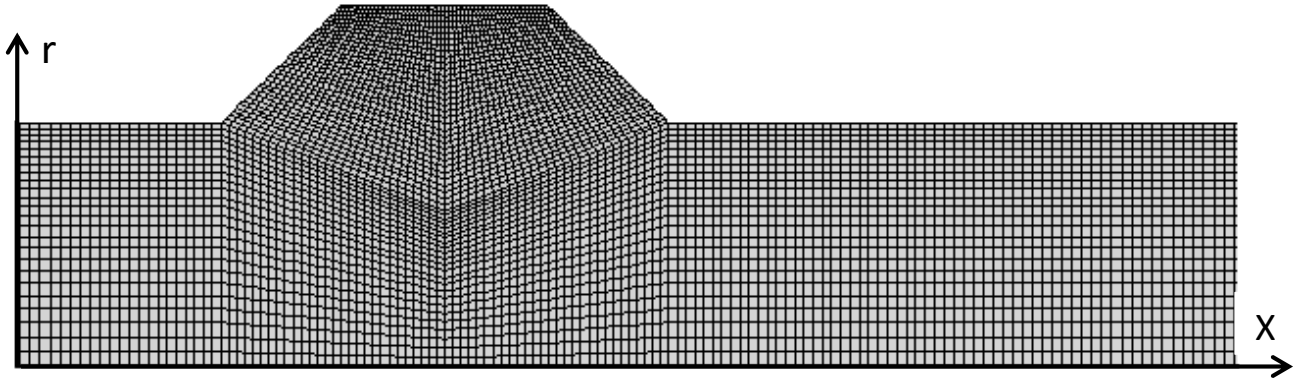

Figure 09: Discretization of the computational domain (for Aneurysm)

. The computational results with quadrilateral shaped grid has been shown in the table below.

Table 01: Grid Independency test for stenosis and aneurysm

stenosis				aneurysm			
32%(depth=.8mm)		48%(depth=1.2mm)		32%(depth=.8mm)		48%(depth=1.2mm)	
Elements number	Central axial velocity	Elements number	Central axial velocity	Elements number	Central axial velocity	Elements number	Central axial velocity
10120	.83	10724	1.32	10920	.539	11428	.5282
19035	.901	19206	1.48	19440	.556	19986	.549
28458	.9180	29244	1.52	32585	.569	34264	.568
41778	.9183	41826	1.521	42636	.569	44426	.5693
50592	.9183	50976	1.521	51648	.569	52400	.5693
65035	.9183	65632	1.521	66586	.569	68564	.5693

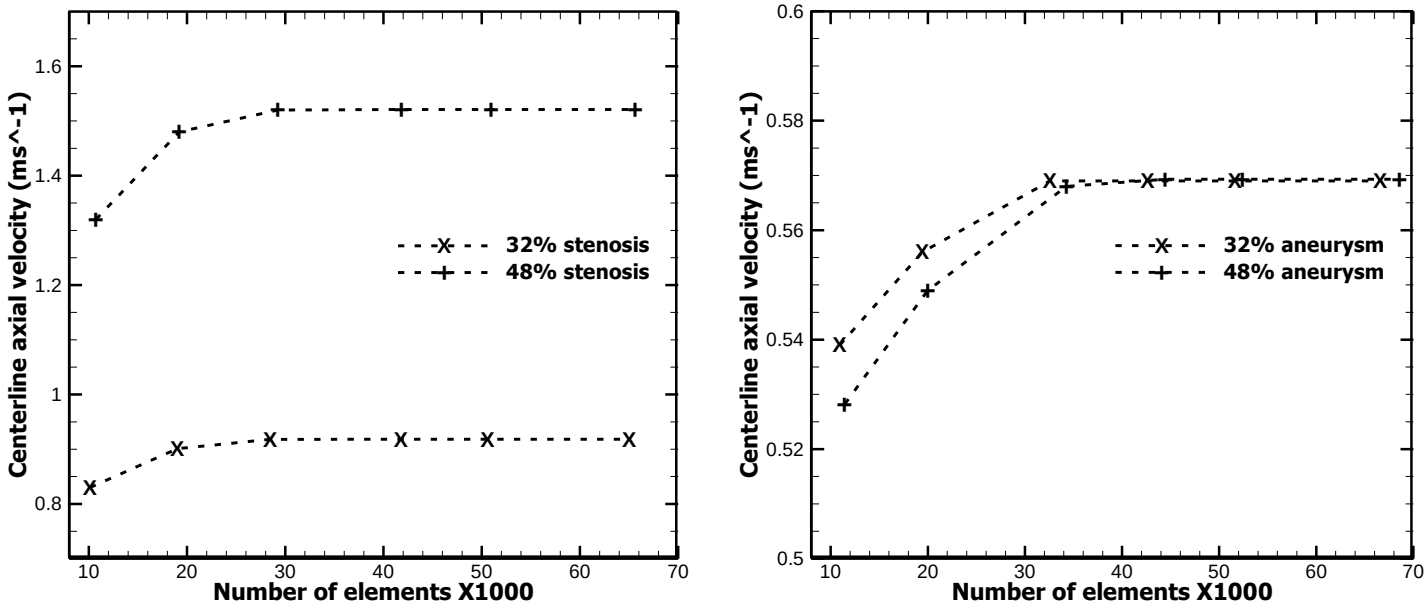

(a) stenosis **(b) aneurysm**

Figure10: Grid Independency Test for (a) stenosis and (b) aneurysm

2.5 Boundary conditions in the present computation:

- **At inlet:**

  'velocity inlet' boundary is used. The same sinusoidal volume flow as in Ojha et al.[19] is used but with a phase shift of 128^0(123miliseconds). The velocity is found out by dividing the volume flow rate with the area.

$$Q = 4.3+2.6 \sin\left(\frac{2\pi t}{T}\right)$$

$$V_{inlet} = \frac{Q}{Area}$$

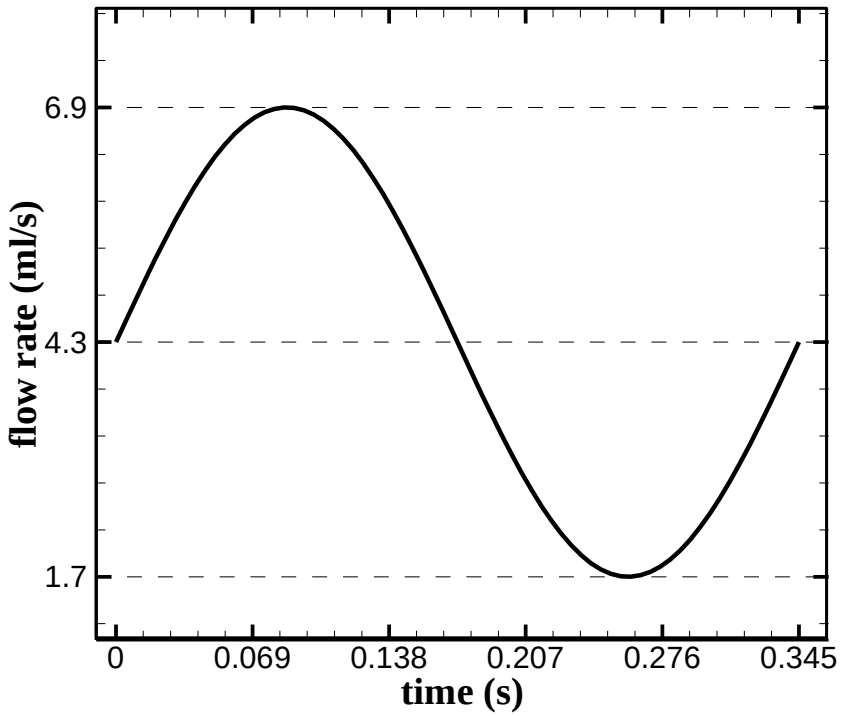

Figure 11: Sinusoidal Volume flow at inlet

- **At outlet:**

  At outlet, the flow is considered fully developed. Zero normal gradient for all flow variables except pressure is considered as well.'Outflow' boundary condition is used which satisfies, $\frac{\partial \boldsymbol{u}_r}{\partial x} = \frac{\partial \boldsymbol{u}_x}{\partial x} = 0$.

- **At centerline:**

  x axis has been considered as the axial symmetry condition.

- **At wall:**

  No slip boundary with no flow: $u_x = u_r = 0$.

2.6 Validation of CFD code

To prove the acceptance of the numerical result, the results should be compared with the solutions that were done before and widely accepted. As our work is unsteady pulsatile laminar flow, so, our simulated results are compared with the experimental data obtained by Ojha et al.[19], that also considered same conditions. The model of ojha et al.[19] is shown in figure 06, where , $\theta_1=30^0$ and $\theta_2=45^0$ and L=1.5mm. Time dependent centerline velocity distribution at different distal positions of the stenosis: Z' = 1, 2.5, 4.3 where Z' is taken as the normalized distance from the centre of the stenosis and it is expressed as Z' =Z/D, where, D is the diameter and Z is the axial distance of the point from the middle point of the stenosis in axis line. The pulsatile fow has a time averaged flow of 4.3 ml/s with a sinusoidal flow of 2.9 Hz frequency having an amplitude of 2.6 ml/s. 2.9 Hz frequency is equivalent to 345 ms of Time Period. The fluid density of .755 g/cm^3 and viscosity of 1.43 cP have been used which corresponds to the property of Deoderized Kerosen (shell-shol 715) at temperature of 20 ^{0}C. For the Newtonian assumption of the blood, the flow characteristic of the fluid (Kerosene) will be similar: for the same dimensionless number, Reynolds number. The Reynolds number considers the constriction free inner diameter of the artery, time-averaged mean velocity and constant viscosity for Newtonian behavior. Reynolds number is expressed as Re =VD/γ. The pulse applied at the inlet of the artery indicates a certain Womersley number. Womersley number indicates how is the transient inertial effect compared to the viscous effects and this number does not affect the Reynolds number. Here womerseley number is 7.75. The applied pulse corresponds to the mean Reynolds Number of 578 with a highest and lowest number of 928 and 228 respectively and it is shown in figure 12.

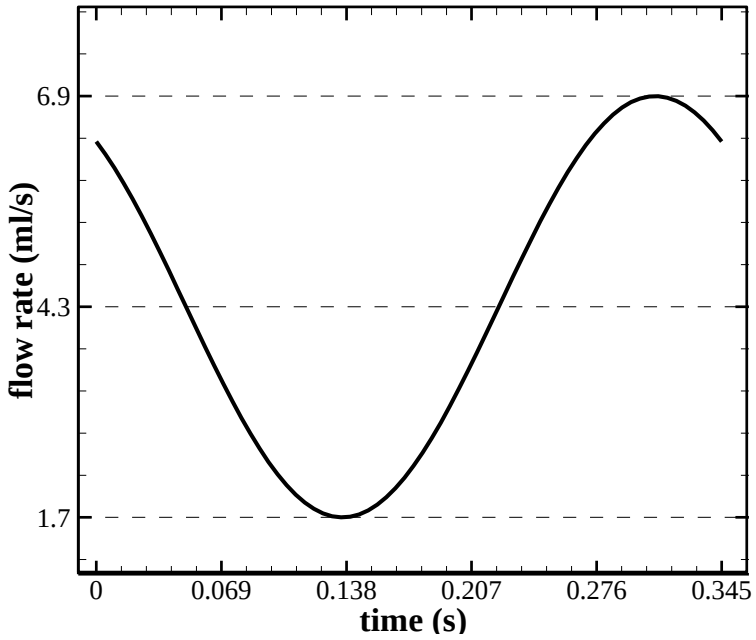

Figure 12: Volumetric flow at the inlet of the artery in the simulation and that of Ojha et al.[19]

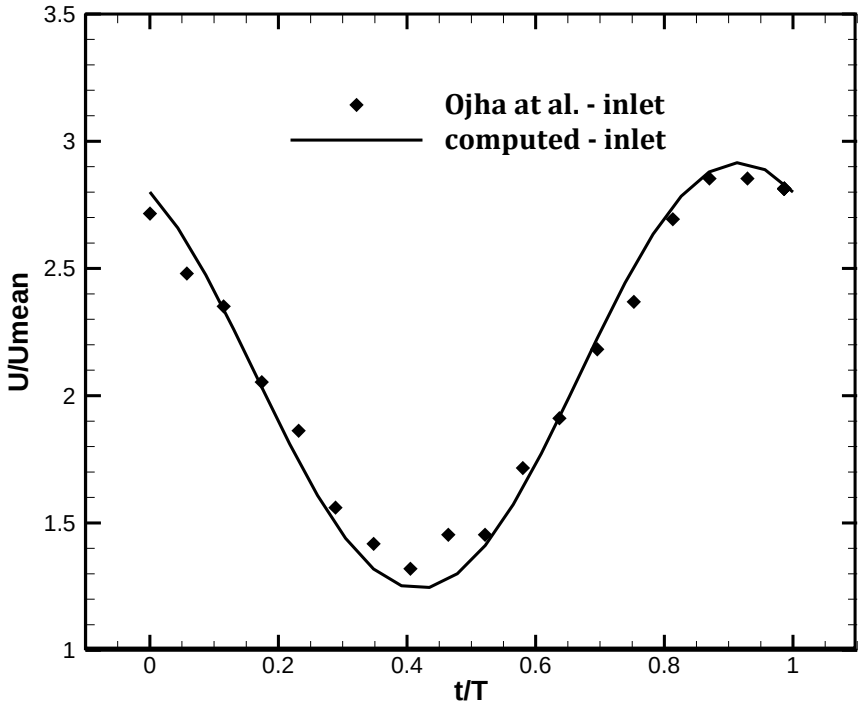

Figure 13: Inlet Centerline Velocity Profile

Before comparing velocity distribution different distal points of the stenosis, centerline time varying/time dependent velocity is compared just at the inlet of the stenosis, in **figure 13**. It can be seen that velocities are similar throughout except at the beginning and the end portion. This little difference in the velocity causes discrepancy in the experimental and simulated results.

The experimental time varying velocity at different distal points has been compared with the results obtained from the simulation. There is a slight error at the end of the period but the error is negligible and the numerical calculation is acceptable.

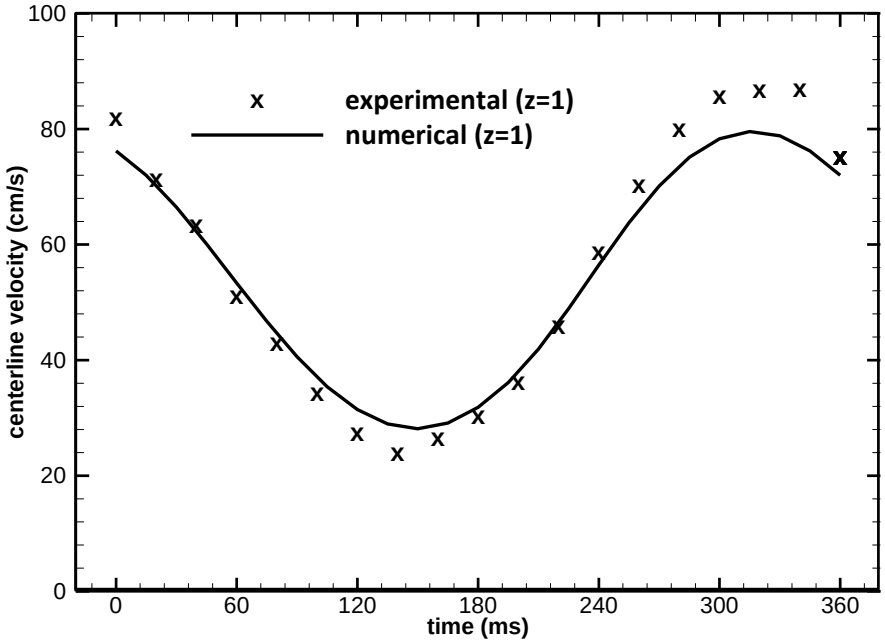

Figure 14: Centerline axial velocity at Z'=1

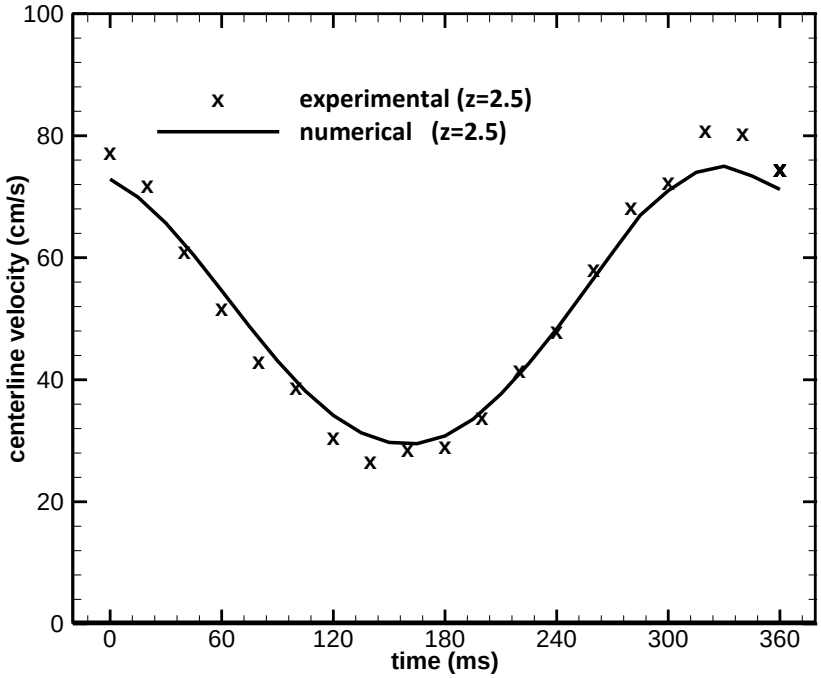

Figure 15: Centerline axial velocity at Z'=2.5

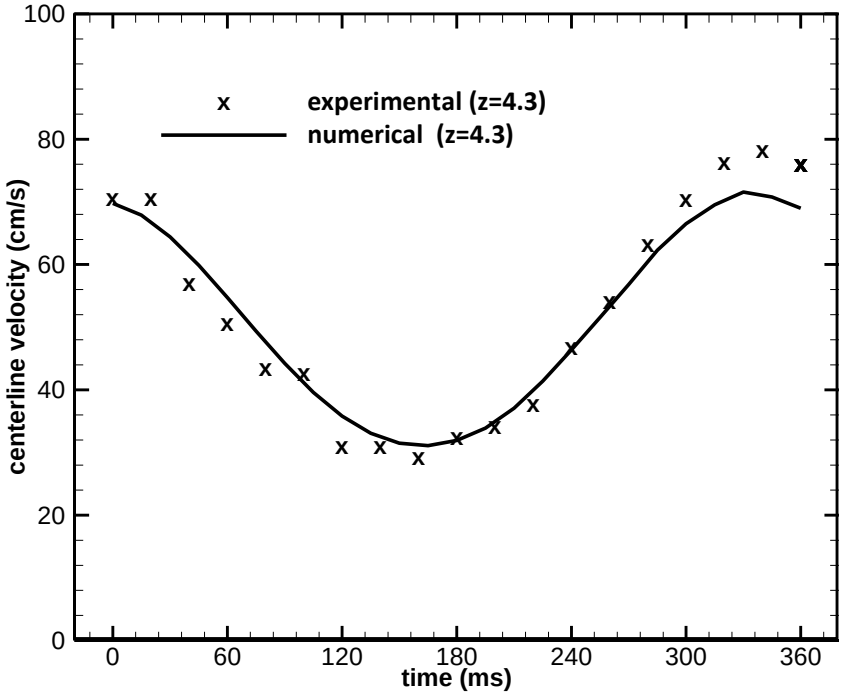

Figure16: Centerline axial velocity at Z'=4.3

3 Results and Discussions

Fluctuating flow, with its effects, through the modeled arterial stenosis and arterial aneurysm will be discussed in detail here. Predominantly, the presence of arterial stenosis and arterial aneurysm of the same strength will be presented and compared to find out the relatively dangerous one. To do so, radial velocity distribution at different arterial locations and also wall shear stress have considered as the parameters. In each sections the effects are presented for two flow frequencies: Wo=7.75, Wo=10. In total, two different sizes of both stenosis and aneurysm are shown: severity of 32% and severity of 48%. The model of the stenosis is the same as that of Ojha et al. except that the upstream angle of the stenosis has an angle of 45^0. And the flow sinusoid is similar to that of Ojha et al. with a slight difference in the flow beginning. The present flow has a mean flow of 4.3 ml/s and amplitude of 2.6 ml/s as shown in figure 10 and the flow began at angle of 0^0 whereas, in the model of Ojha et al., the flow started at 123^0.

3.1 Radial velocity Comparison between 32% stenosis and 32% aneurysm

3.1.1 Radial velocity distribution in the flow field at Wo=7.75

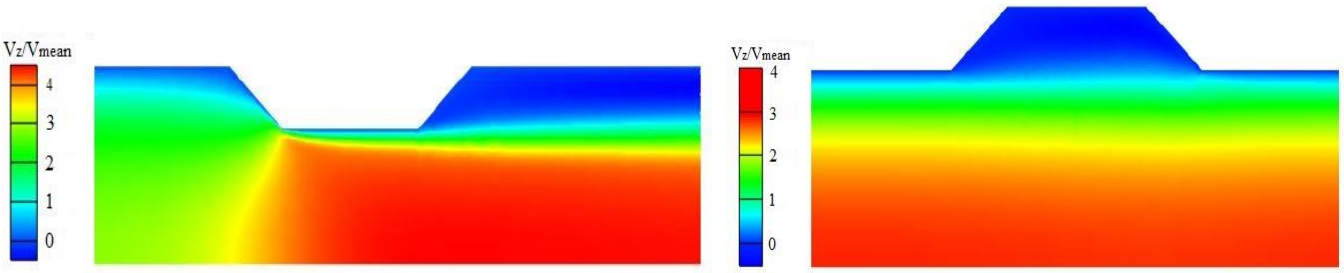

(a) **(b)**

Figure 17: Radial velocity distribution at t/T=0.25 through (a) stenosis and (b) aneurysm, for 32%

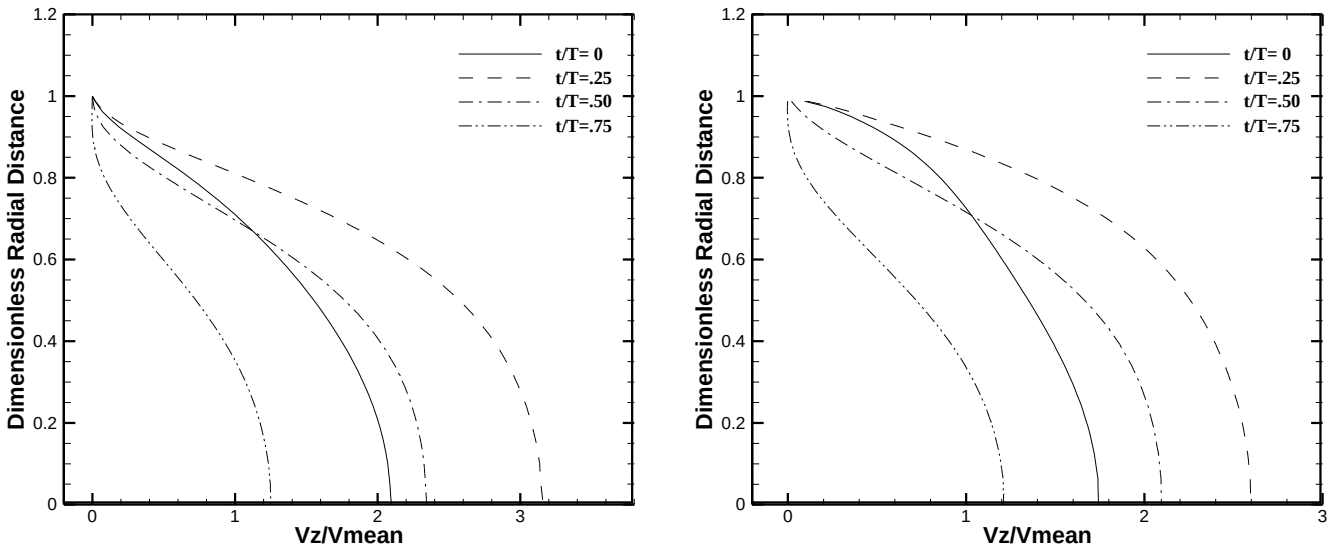

(a) **(b)**

Figure 18: Instantaneous radial velocity distribution at four key flow time for at just inlet of the (a)stenosis and (b) aneurysm

Here in figure 18, for the stenosis and aneurysm strength of 32%, the flow disturbances created in the just inlet section of the stenosis and aneurysm are presented. The axial velocity profiles are at this section is different from the usual parabolic velocity profile. Though it is at the inlet section of the stenosis and the aneurysm, the profile/flow is affected as the flow is about to contract in stenosis and expand in the aneurysm at smaller and higher flow areas respectively. In both of the stenosis and aneurysm, at the beginning of the pulsatile flow, at t/T=0, the centerline velocity is a bit higher, about 2.1 times and 1.75 times of the steady flow/mean velocity for stenosis and aneurysm respectively. At t/T=0.25 for the maximum flow, the centerline velocities are 3.18 times and 2.6 times of the mean velocity respectively. At t/T=0.50, the centerline velocities are 2.35 times and 2.1 times of the mean flow for stenosis and aneurysm respectively. But region from the wall upto .25 times the radial distance of the artery is found where velocity is always lower than the steady velocity distribution for the stenosis and for stenosis it is only .15 times implying that closer to the wall the velocities in the stenosis are reduced more than in the aneurysm because of the reason that at just inlet the flow is a bit restricted because of the upstream stenosis but for the aneurysm no such restriction is there as the flow is going to be expanded in the upstream aneurysm. At t/T=.75 for the minimum flow, the centerline velocities are 1.22 times and 1.2 times of the mean velocity. In every key points, closer to the centerline, the velocities in the stenosis are higher with respect to that of the aneurysm. It’s because, for stenosis the flow is about to be narrowed in the stenosis at lower area increasing the velocity and for the aneurysm the flow is about to expand in the aneurysm at higher flow area reducing the velocity.

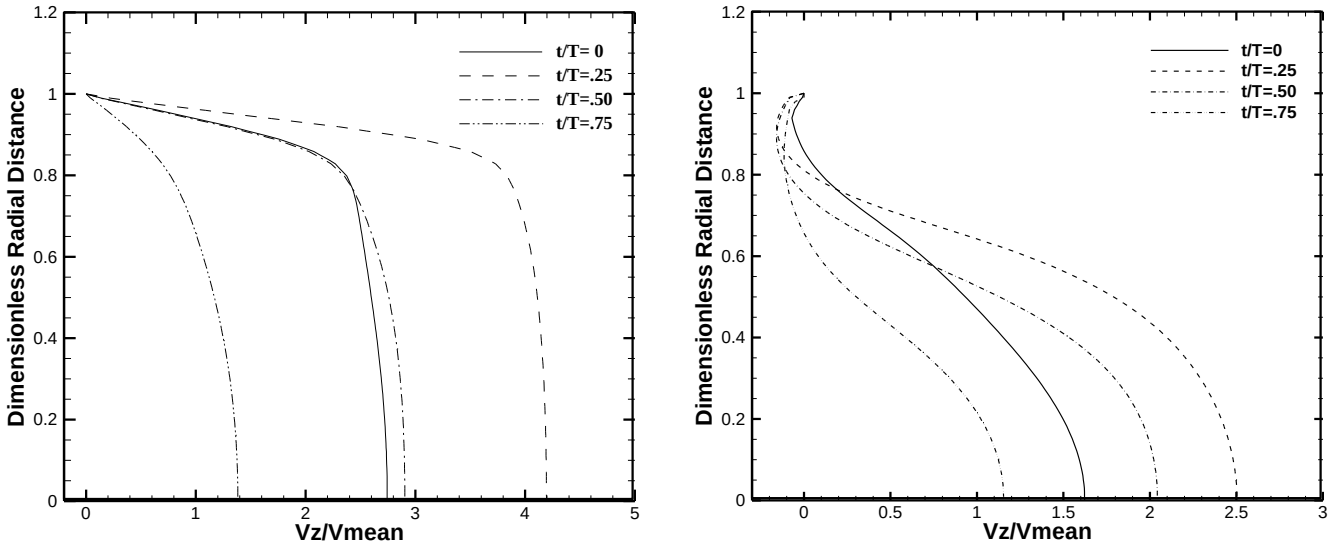

Figure 19: Instantaneous radial velocity distribution at four key flow times at Throat of the (a) stenosis and (b) aneurysm

Here in figure 19, it shows the velocity distribution at the throat of the stenosis and aneurysm at different time steps. In this region, in the stenosis, the fluid accelerates and velocity reaches its maximum values, whereas, in the aneurysm, the fluid decelerates, because of the high flow areas, to the minimum values. Velocity profile for the stenosis becomes flattened indicating very high values compared to the steady velocity distribution. Flattened velocity distribution of the stenosis results in the thinning of the boundary layer. But for the aneurysm, the deflated velocity distribution results in the widening of the boundary layer. In the stenosis and aneurysm, at the beginning of the pulsatile flow, at t/T=0, the centerline velocities are 2.75 times and 1.65 times of the steady flow/mean velocity for stenosis and aneurysm respectively. At t/T=0.25 for the maximum flow, the centerline velocities are 4.2 times and 2.5 times of the mean velocity respectively. At t/T=0.50, the centerline velocities are 2.9 times and 2.05 times of the mean flow for stenosis and aneurysm respectively. At t/T=.75 for the minimum flow, the centerline

velocities are 1.38 times and 1.15 times of the mean velocity. In every key points, the velocities in the stenosis are much higher with respect to that of the aneurysm.

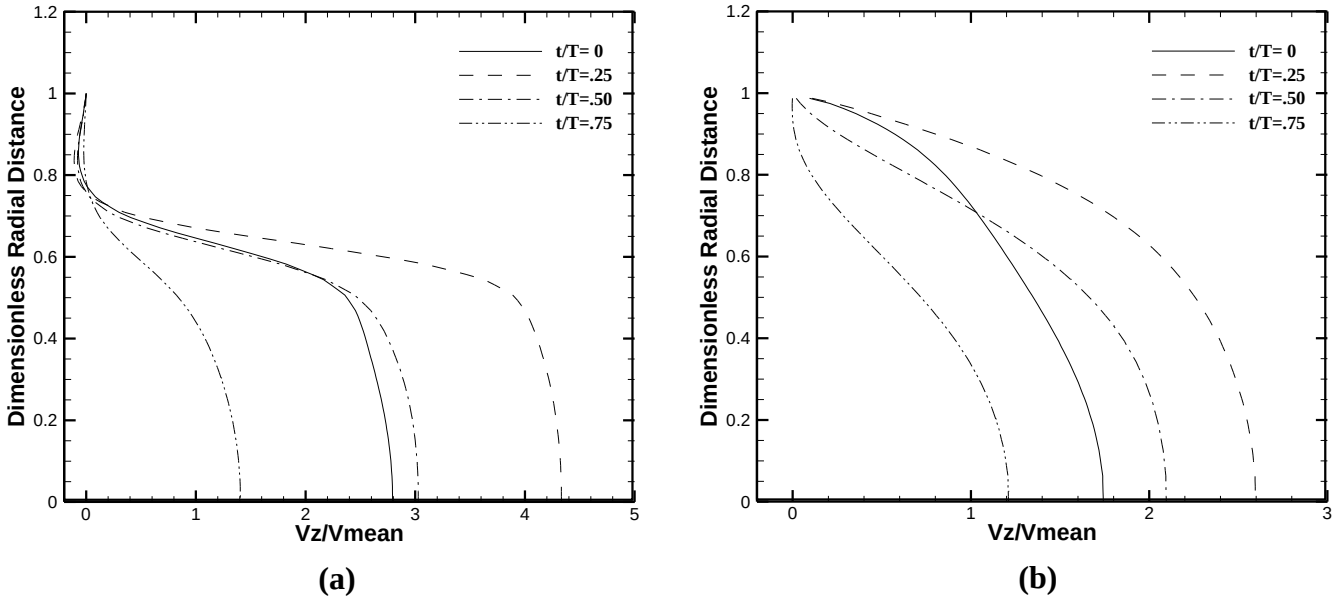

Figure 20: Instantaneous radial velocity distribution at four key flow times at Just Outlet of the (a) stenosis and (b) aneurysm

Here in figure 20, it shows the velocity distribution at Just Outlet of the stenosis and aneurysm at different time steps. Just at the outlet of the stenosis, because of the abrupt rise of the area, the flow greatly slows down developing a possible boundary layer separation near the wall as shown in figure, and the velocity is high near the center positions. The velocity distribution for all the time points shows a region where flow becomes close to zero. This region is 0.3 times the radius of the artery from the side of the wall and after this region flattened velocity profile is seen. But the cases are completely different for the aneurysm, showing the velocity profiles almost the same as the just inlet section of the aneurysm. The aneurysm didn't have considerable change on

the velocity distribution at the inlet and outlet sections of the aneurysm. And finally, closer to the centerline, the velocities are much higher in stenosis than in aneurysm.

3.1.2 Radial velocity distribution in the flow field at Wo=10

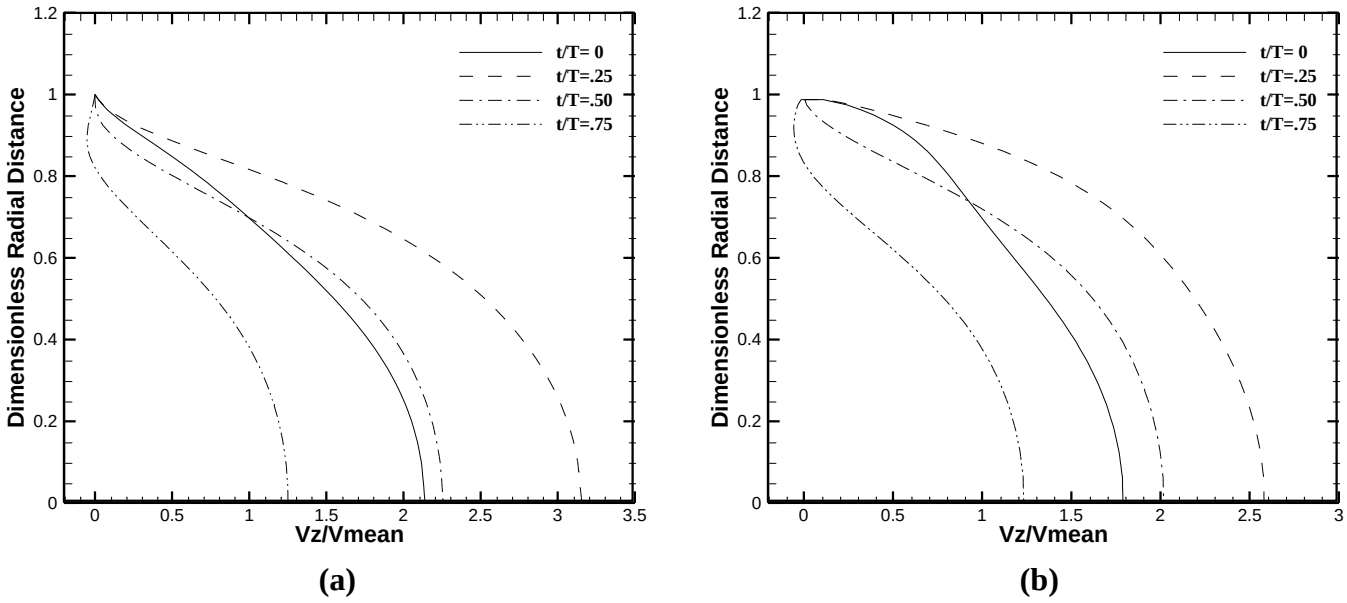

Figure 21: Instantaneous radial velocity distribution at four key flow time for at just inlet of the (a)stenosis and (b) aneurysm

Here in fig 21, for the stenosis and aneurysm strength of 32%, with a flow having the Wo=10, the flow disturbances created in the just inlet section of the stenosis and aneurysm have been shown. The axial velocity profiles are at this section is different from the usual parabolic velocity profile. Though it is at the inlet section of the stenosis and the aneurysm, the profile/flow is affected as the flow is about to contract in stenosis and expand in the aneurysm at smaller and higher flow areas respectively. In both of the stenosis and aneurysm, at the beginning of the

pulsatile flow, at t/T=0, the centerline velocity is a bit higher, about 2.12 times and 1.8 times of the steady flow/mean velocity for stenosis and aneurysm respectively. At t/T=0.25 for the maximum flow, the centerline velocities are 3.15 times and 2.6 times of the mean velocity respectively. At t/T=0.50, the centerline velocities are 2.25 times and 2.0 times of the mean flow for stenosis and aneurysm respectively. But region from the wall up to .30 times the radial distance of the artery is found where velocity is always lower than the steady velocity distribution for the stenosis and for stenosis it is only .20 times implying that closer to the wall the velocities in the stenosis are reduced more than in the aneurysm because of the reason that at just inlet the flow is a bit restricted because of the upstream stenosis but for the aneurysm no such restriction is there as the flow is going to be expanded in the upstream aneurysm. At t/T=.75 for the minimum flow, the centerline velocities are 1.25 times and 1.22 times of the mean velocity. In every key points, closer to the centerline, the velocities in the stenosis are higher with respect to that of the aneurysm. It's because, for stenosis the flow is about to be narrowed in the stenosis at lower area increasing the velocity and for the aneurysm the flow is about to expand in the aneurysm at higher flow area reducing the velocity.

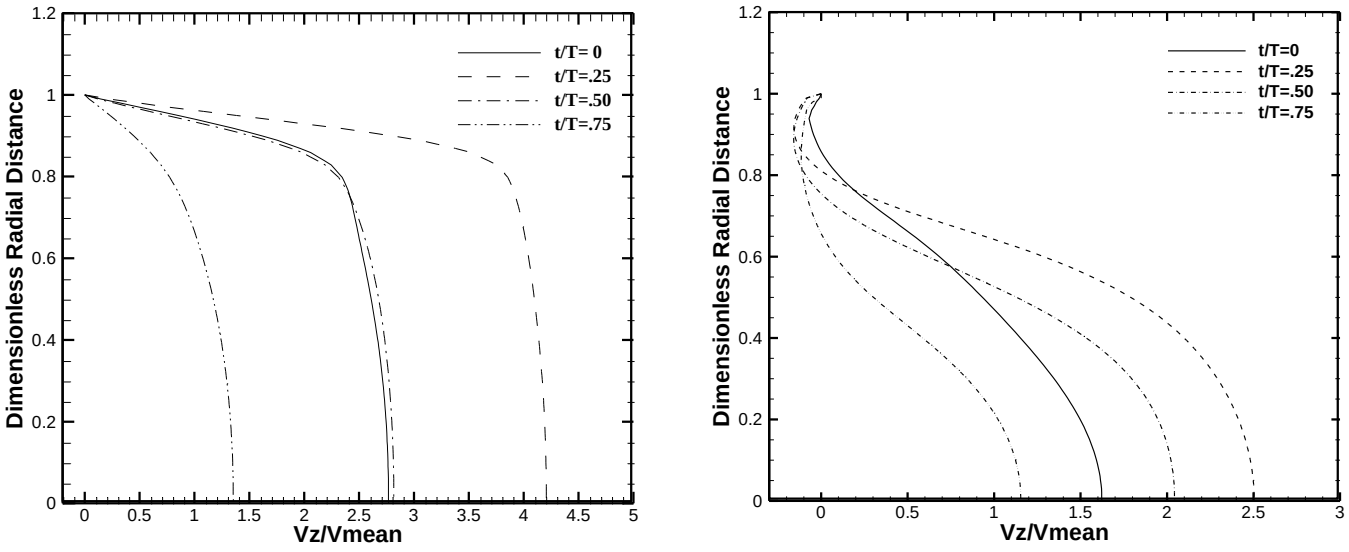

Figure 22: Instantaneous radial velocity distribution at four key flow time for at Throat of the (a)stenosis and (b) aneurysm

Here in figure 22, it shows the velocity distribution at the throat of the stenosis and aneurysm at different time steps for the Wo=10. In this region, in the stenosis, the fluid accelerates and velocity reaches its maximum values, whereas, in the aneurysm, the fluid decelerates, because of the high flow areas, to the minimum values. Velocity profile for the stenosis becomes flattened indicating very high values compared to the steady velocity distribution. Flattened velocity distribution of the stenosis results in the thinning of the boundary layer. But for the aneurysm, the deflated velocity distribution results in the widening of the boundary layer. In the stenosis and aneurysm, at the beginning of the pulsatile flow, at t/T=0, the centerline velocities are 2.76 times and 1.63 times of the steady flow/mean velocity for stenosis and aneurysm respectively. At t/T=0.25 for the maximum flow, the centerline velocities are 4.2 times and 2.51 times of the mean velocity respectively. At t/T=0.50, the centerline velocities are 2.8 times and 2.03 times of the mean flow for stenosis and aneurysm respectively. At t/T=.75 for the minimum flow, the

centerline velocities are 1.35 times and 1.16 times of the mean velocity. In every key points, the velocities in the stenosis are much higher with respect to that of the aneurysm.

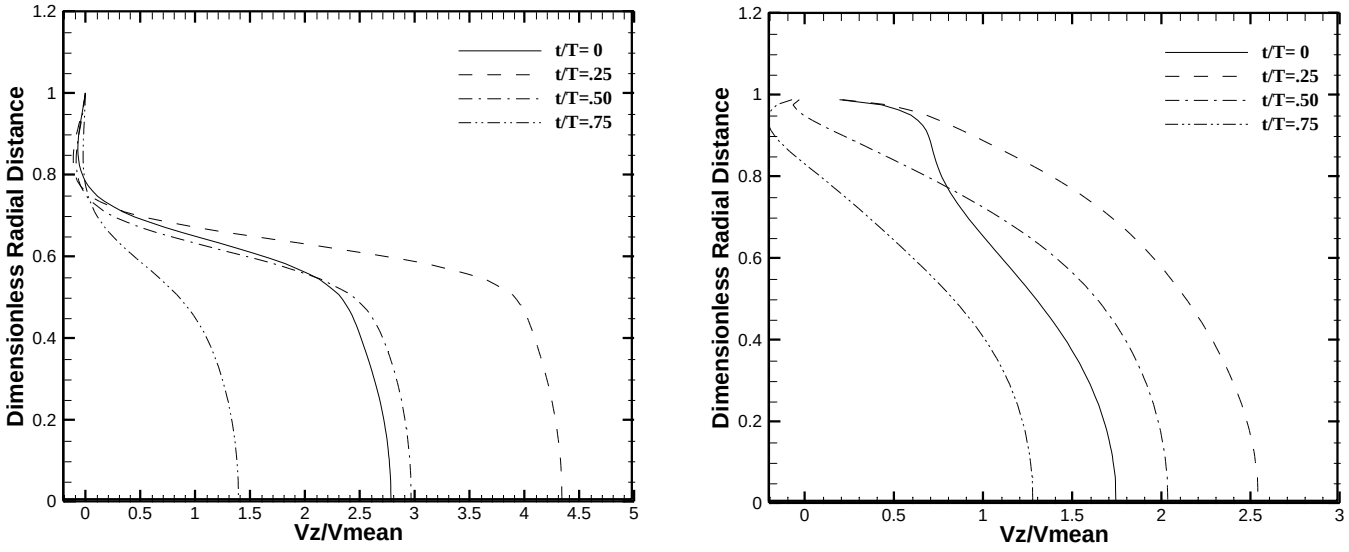

Figure 23: Instantaneous radial velocity distribution at four key flow time for at Just Outlet of the (a)stenosis and (b) aneurysm

Here in figure 23, it shows the velocity distribution at Just Outlet of the stenosis and aneurysm at different time steps for the Wo=10. Just at the outlet of the stenosis, because of the abrupt rise of the area, the flow greatly slows down developing a possible boundary layer separation near the wall. And, there is rise in the velocity near the center points as the maximum flow is through the central positions because of the creation of the boundary layer near the walls. The velocity distribution for all the time points shows a region where flow becomes close to zero. This region is 0.3 times the radius of the artery and after this region flattened velocity profile is seen. But the cases are completely different for the aneurysm, showing the velocity profiles almost the same as the just inlet section of the aneurysm. The aneurysm didn't have considerable change on the velocity distribution at the inlet and outlet sections of the aneurysm. And finally, closer to the centerline, the velocities are much higher in stenosis than in aneurysm.

3.2 Radial velocity Comparison between 48% stenosis and 48% aneurysm

3.2.1 Radial velocity distribution in the flow field Wo=7.75

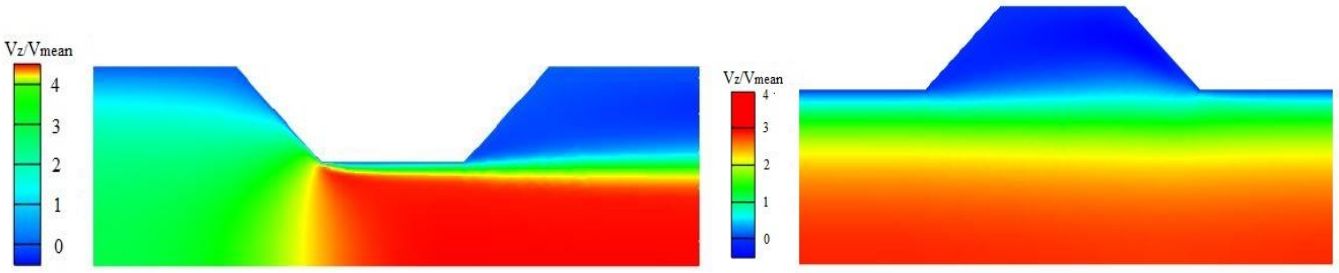

(a) **(b)**

Figure 24: Radial velocity distribution at t/T=0.25 through (a) stenosis and (b) aneurysm, for 48% severity

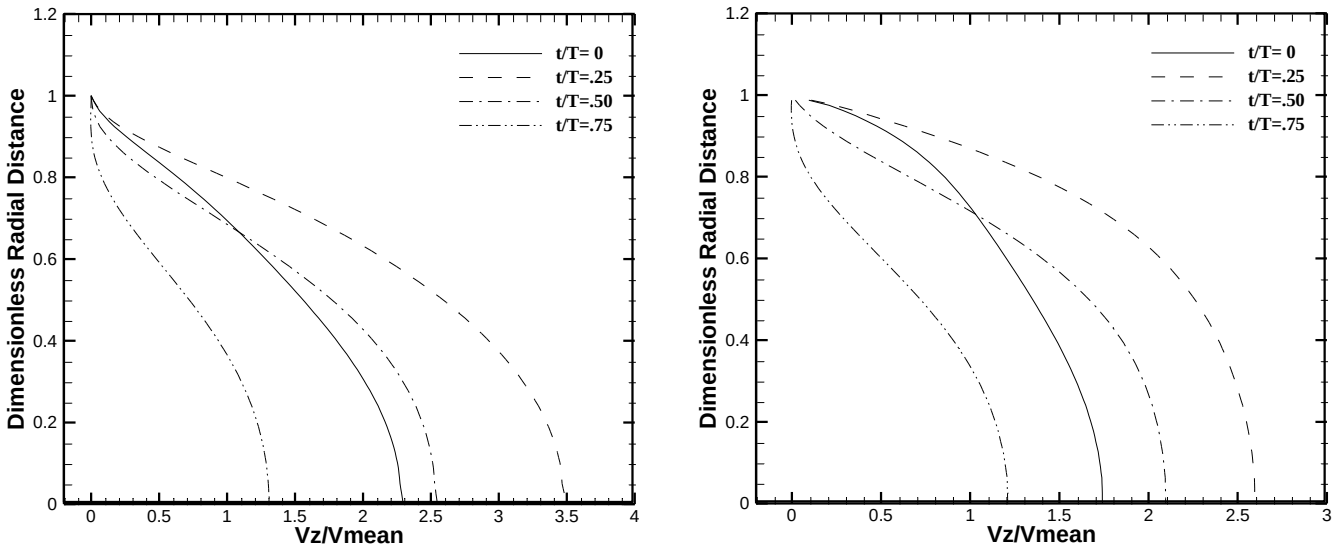

(a) **(b)**

Figure 25: Instantaneous radial velocity distribution at four key flow time for at Just Inlet of the (a)stenosis and (b) aneurysm

Here in figure 25, for the stenosis and aneurysm strength of 48%, with a flow having the Wo=7.75, the flow disturbances created in the just inlet section of the stenosis and aneurysm have been shown. The axial velocity profiles are at this section is different from the usual parabolic velocity profile. Though it is at the inlet section of the stenosis and the aneurysm, the profile/flow is affected as the flow is about to contract in stenosis and expand in the aneurysm at smaller and higher flow areas respectively. In both of the stenosis and aneurysm, at the beginning of the pulsatile flow, at t/T=0, the centerline velocity is a bit higher, about 2.3 times and 1.75 times of the steady flow/mean velocity for stenosis and aneurysm respectively. At t/T=0.25 for the maximum flow, the centerline velocities are 3.5 times and 2.6 times of the mean velocity respectively. At t/T=0.50, the centerline velocities are 2.55 times and 2.10 times of the mean flow for stenosis and aneurysm respectively. But region from the wall up to .27 times the radial distance of the artery is found where velocity is always lower than the steady velocity distribution for the stenosis and for stenosis it is only .25 times. At t/T=.75 for the minimum flow, the centerline velocities are 1.3 times and 1.20 times of the mean velocity. In every key points, closer to the centerline, the velocities in the stenosis are higher with respect to that of the aneurysm. It's because, for stenosis the flow is about to be narrowed in the stenosis at lower area increasing the velocity and for the aneurysm the flow is about to expand in the aneurysm at higher flow area reducing the velocity.

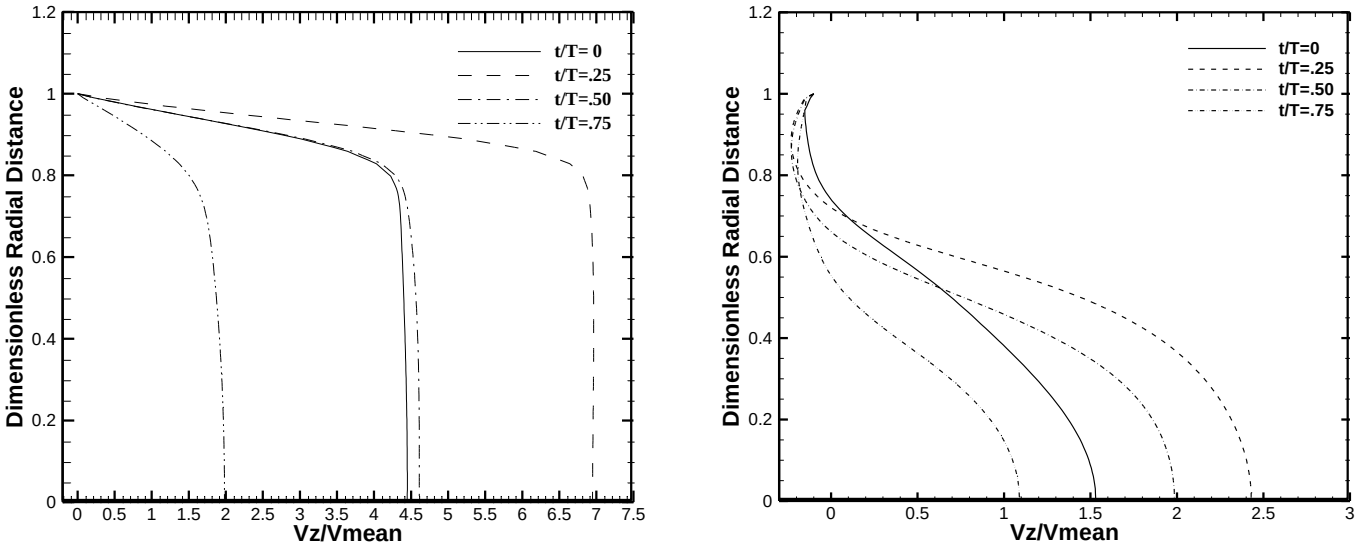

Figure 26: Instantaneous radial velocity distribution at four key flow time for at Throat of the (a)stenosis and (b) aneurysm

Here in figure 26, it shows the velocity distribution at the throat of the stenosis and aneurysm at different time steps for the Wo=7.75. In this region, in the stenosis, the fluid accelerates very sharply and velocity reaches its maximum values, whereas, in the aneurysm, the fluid decelerates, because of the high flow areas, to the minimum values. Velocity profile for the stenosis becomes flattened, very high velocity gradient develops up to 0.1 times the radius of the artery width and this phenomenon indicates very high values towards the center, compared to the steady velocity distribution. Flattened velocity distribution of the stenosis results in the thinning of the boundary layer. But for the aneurysm, the deflated velocity distribution results in the widening of the boundary layer. In the stenosis and aneurysm, at the beginning of the pulsatile flow, at t/T=0, the centerline velocities are 4.42 times and 1.53 times of the steady flow/mean velocity for stenosis and aneurysm respectively. At t/T=0.25 for the maximum flow, the centerline velocities are 6.95 times and 2.42 times of the mean velocity respectively. At

t/T=0.50, the centerline velocities are 4.6 times and 2.0 times of the mean flow for stenosis and aneurysm respectively. At t/T=.75 for the minimum flow, the centerline velocities are 1.95 times and 1.1 times of the mean velocity. In every key points, the velocities in the stenosis are too much higher with respect to that of the aneurysm. Because of high depth of the stenosis, the smaller flow area resulted in the increase of velocity in the stenotic artery. Whereas, due to expansion of flow area there is reduction of the velocities.

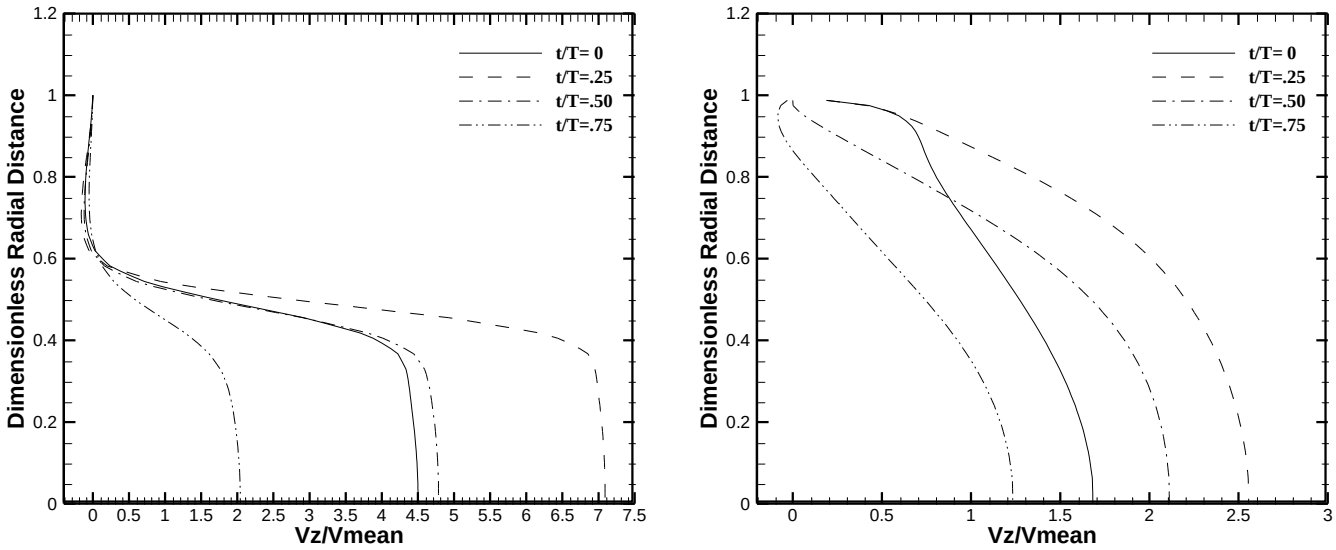

Figure 27: Instantaneous radial velocity distribution at four key flow time for at Just Outlet of the (a)stenosis and (b) aneurysm

Here in figure 27, it shows the velocity distribution at Just Outlet of the stenosis and aneurysm at different time steps for the Wo=7.75. Just at the outlet of the stenosis, because of the abrupt rise of the area, the flow greatly slows down developing a possible boundary layer separation near the walls but the velocity is observed to increase towards the centerline. The velocity distribution for all the time points shows a region where flow becomes close to zero. This region is 0.50

times the radius of the artery and after this region flattened velocity profile is seen. But the cases are completely different for the aneurysm, showing the velocity profiles almost the same as the just inlet section of the aneurysm. The aneurysm didn't have considerable change on the velocity distribution at the inlet and outlet sections of the aneurysm. And finally, closer to the centerline, the velocities are much higher in stenosis than in aneurysm.

3.2.2 Radial velocity distribution in the flow field at Wo=10

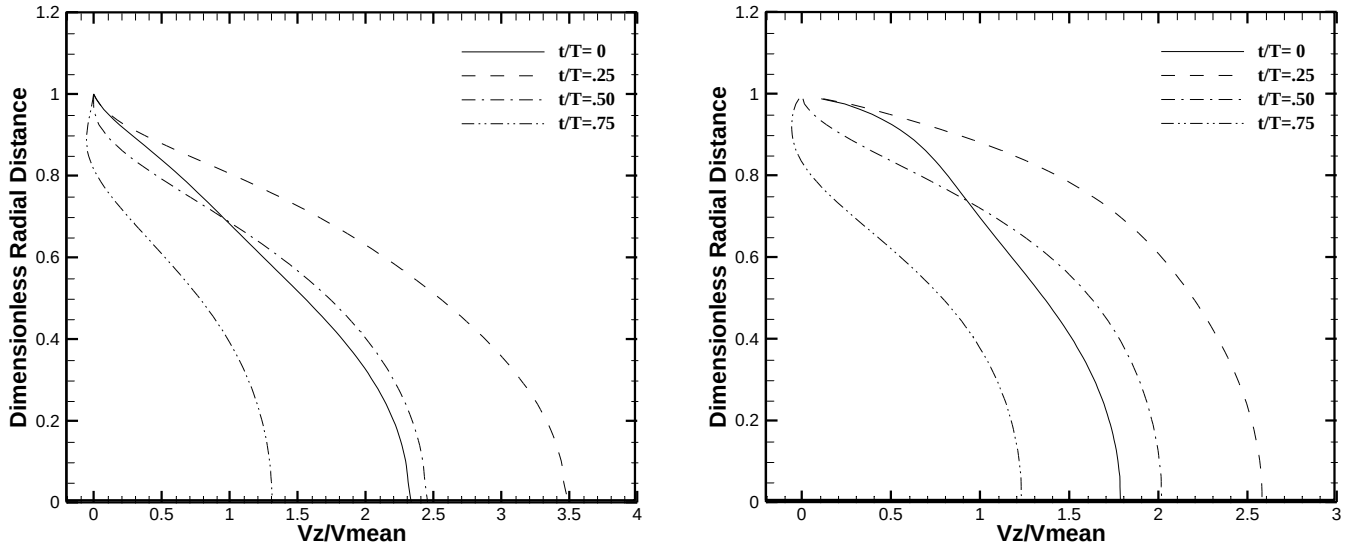

Figure 28: Instantaneous radial velocity distribution at four key flow time for at Just Inlet of the (a)stenosis and (b) aneurysm

Here in fig 28, for the stenosis and aneurysm strength of 48%, with a flow having the Wo=10, the flow disturbances created in the just inlet section of the stenosis and aneurysm have been shown. The axial velocity profiles are at this section is different from the usual parabolic velocity

profile. Though it is at the inlet section of the stenosis and the aneurysm, the profile/flow is affected as the flow is about to contract in stenosis and expand in the aneurysm at smaller and higher flow areas respectively. In both of the stenosis and aneurysm, at the beginning of the pulsatile flow, at t/T=0, the centerline velocity is a bit higher, about 2.32 times and 1.78 times of the steady flow/mean velocity for stenosis and aneurysm respectively. At t/T=0.25 for the maximum flow, the centerline velocities are 3.48 times and 2.58 times of the mean velocity respectively. At t/T=0.50, the centerline velocities are 2.45 times and 2.0 times of the mean flow for stenosis and aneurysm respectively. But region from the wall up to .25 times the radial distance of the artery is found where velocity is always lower than the steady velocity distribution for the stenosis and for stenosis it is only .20 times. At t/T=.75 for the minimum flow, the centerline velocities are 1.3 times and 1.22 times of the mean velocity. In every key points, closer to the centerline, the velocities in the stenosis are higher with respect to that of the aneurysm. It's because, for stenosis the flow is about to be narrowed in the stenosis at lower area increasing the velocity and for the aneurysm the flow is about to expand in the aneurysm at higher flow area reducing the velocity.

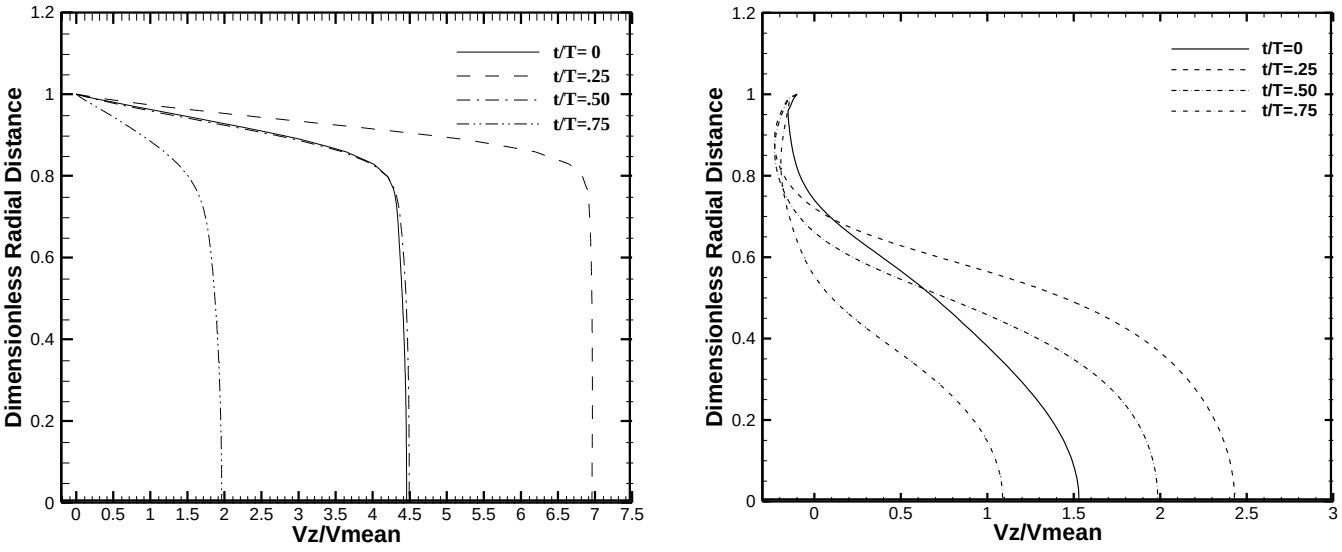

Figure 29: Instantaneous radial velocity distribution at four key flow time for at Throat of the (a)stenosis and (b) aneurysm

Here in figure 29, it shows the velocity distribution at the throat of the stenosis and aneurysm at different time steps for the Wo=10. In this region, in the stenosis, the fluid accelerates very sharply and velocity reaches its maximum values, whereas, in the aneurysm, the fluid decelerates, because of the high flow areas, to the minimum values. Velocity profile for the stenosis becomes flattened, very high velocity gradient develops up to 0.095 times the radius of the artery width and this phenomenon indicates very high values towards the center, compared to the steady velocity distribution. Flattened velocity distribution of the stenosis results in the thinning of the boundary layer. But for the aneurysm, the deflated velocity distribution results in the widening of the boundary layer. In the stenosis and aneurysm, at the beginning of the pulsatile flow, at t/T=0, the centerline velocities are 4.45 times and 1.52 times of the steady flow/mean velocity for stenosis and aneurysm respectively. At t/T=0.25 for the maximum flow, the centerline velocities are 6.95 times and 2.41 times of the mean velocity respectively. At

t/T=0.50, the centerline velocities are 4.5 times and 1.98 times of the mean flow for stenosis and aneurysm respectively. At t/T=.75 for the minimum flow, the centerline velocities are 2.0 times and 1.09 times of the mean velocity. In every key points, the velocities in the stenosis are too much higher with respect to that of the aneurysm. Because of high depth of the stenosis, the smaller flow area resulted in the increase of velocity in the stenotic artery. Whereas, due to expansion of flow area there is reduction of the velocities in the aneurysm. Close to the wall, some irregular velocity profiles are found because of the turbulence created inside the aneurysmal space.

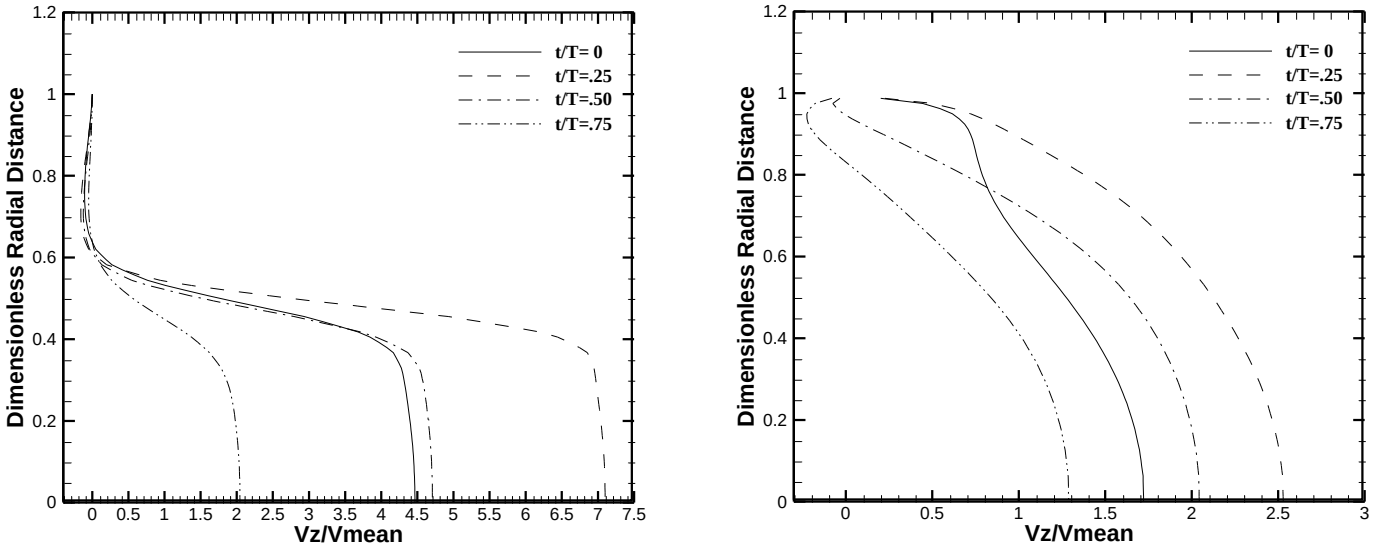

Figure 30: Instantaneous radial velocity distribution at four key flow time for at Just Outlet of the (a)stenosis and (b) aneurysm

Here in figure 30, it shows the velocity distribution at Just Outlet of the stenosis and aneurysm at different time steps for the Wo=10. Just at the outlet of the stenosis, because of the abrupt rise of the area, the flow greatly slows down developing a possible boundary layer separation as shown in figure. It is observed that the velocity towards the centerline increases as the maximum flow

region is the centerline which is the result of thicker boundary layer creation near the walls. The velocity distribution for all the time points shows a region where flow becomes close to zero. This region is 0.50 times the radius of the artery and after this region flattened velocity profile is seen. But the cases are completely different for the aneurysm, showing the velocity profiles almost the same as the just inlet section of the aneurysm. The aneurysm didn't have considerable change on the velocity distribution at the inlet and outlet sections of the aneurysm. And finally, closer to the centerline, the velocities are too much higher in stenosis than in aneurysm.

3.3 WSS Comparison between 32% stenosis and 32% aneurysm

z/D is the dimensionless axial distance where z/D=0 indicates the mid position of the stenosis and aneurysm. Negative values indicate the locations at the left side or upstream side of the stenosis/aneurysm and positive values indicate the downstream side of the stenosis/aneurysm.

3.3.1 WSS at Wo=7.75

Wall shear stress is the determining hemodynamic parameter which will indicate the extent of severity of the stenosis or aneurysm.

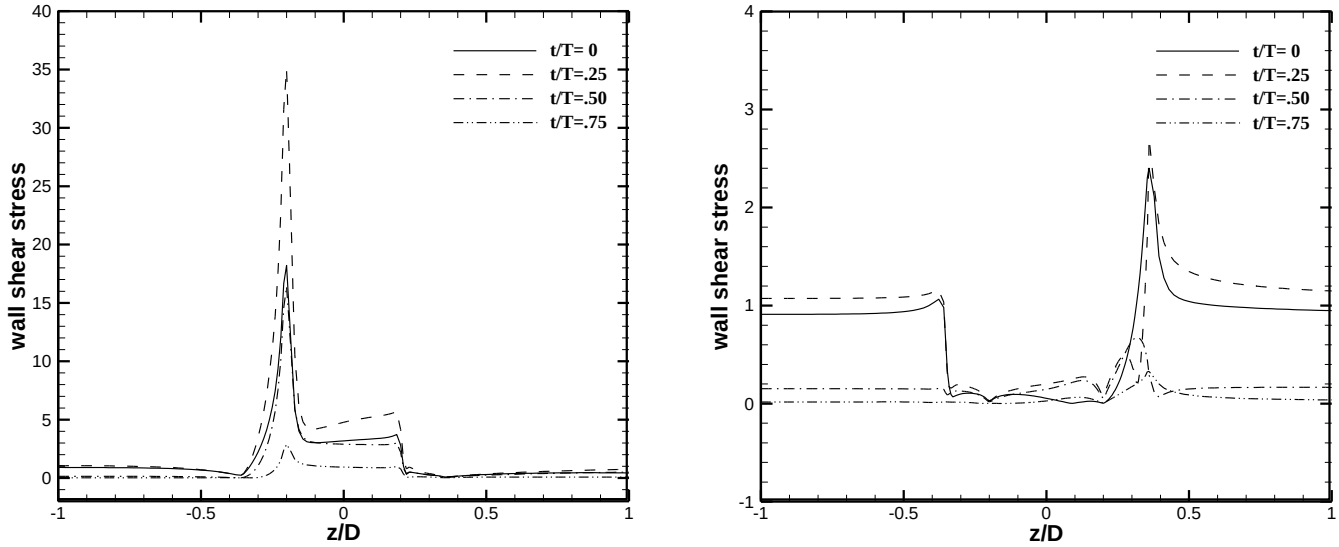

Figure 31: WSS distribution at four key flow time for (a)stenosis and (b) aneurysm

Here, in the figure 31, for the 32% stenosis/aneurysm with a flow having Wo=7.75, the Wall Shear Stress distributions along the axial direction in the wall for different times are presented. It is clearly observed that for the stenosis, the WSS is highest at the inlets sections of the stenosis as the flow is hitting directly to the inlet side of the stenosis causing the abrupt increase of WSS, a bit higher throughout the stenosis area and finally drops down after the outlet sections. But for the aneurysm, the WSS behavior is different from that of stenosis. Here, the maximum WSS is found at the outlet sections of the aneurysm as the flow expanding form the inlet sides hits the outlet side creating high WSS. For the times when the fluid accelerates, the WSS maintains a bit higher value throughout the axial length and finally abruptly reduces and becomes minimum inside the aneurysm as flow is relaxed because of the aneurysmal expansion. At t/T=0, maximum WSS for stenosis and aneurysm are 18 and 2.4 respectively. At t/T=0.25, when the flow quickly accelerates, the maximum WSS for stenosis and aneurysm becomes 35 and 2.6

respectively. At t/T=0.50, the maximum WSS for stenosis and aneurysm becomes 15 and 0.5 respectively. At t/T=0.75, maximum WSS for stenosis and aneurysm are 3 and 0.2 respectively.. Out of all times the maximum WSS is found when the flow accelerates at t/T=0.25. In all the cases, the maximum WSS developed in the stasis is much higher than that developed in aneurysm.

3.3.2 WSS at Wo=10

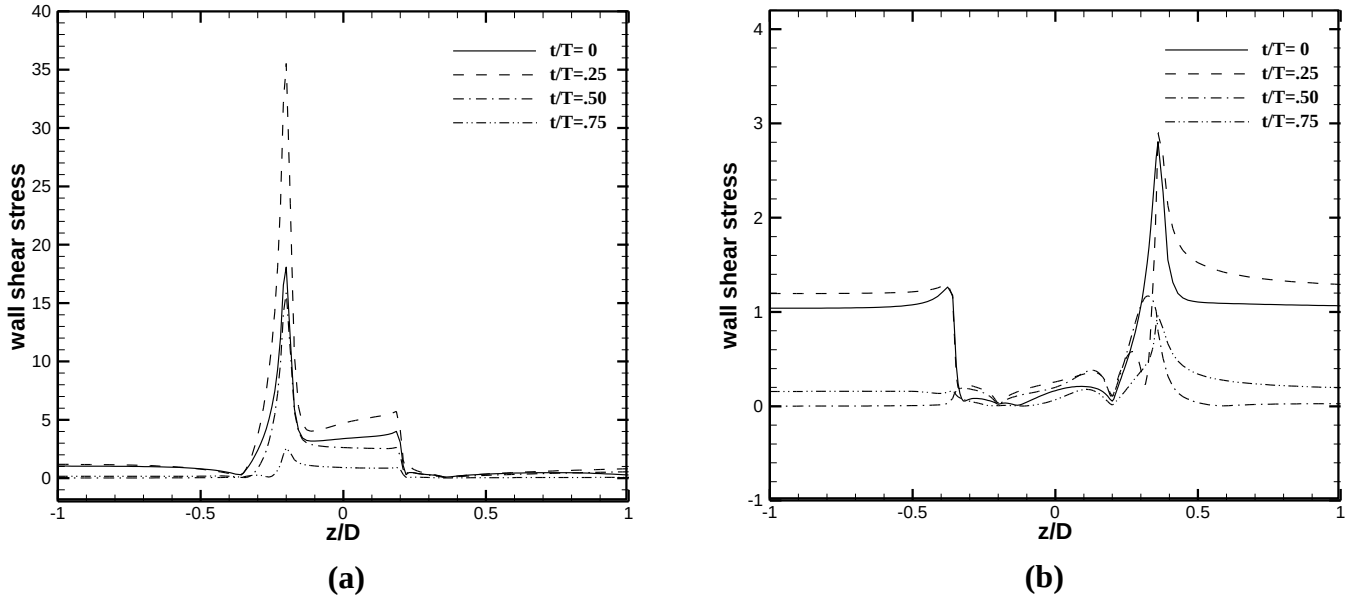

Figure 32: WSS distribution at four key flow time for (a)stenosis and (b) aneurysm

Here, in the figure 32, for the 32% stenosis/aneurysm with a flow having Wo=10, the Wall Shear Stress distributions along the axial direction in the wall for different times are presented. It is clearly observed that for the stenosis, the WSS is highest at the inlets sections of the stenosis as the flow is hitting directly to the inlet side of the stenosis causing the abrupt increase of WSS, a bit higher throughout the stenosis area and finally drops down after the outlet sections. But for the aneurysm, the WSS behavior is different from that of stenosis. Here, the maximum WSS is

found at the outlet sections of the aneurysm as the flow expanding form the inlet sides hits the outlet side creating high WSS. For the times when the fluid accelerates, the WSS maintains a bit higher value throughout the axial length and finally abruptly reduces and becomes minimum inside the aneurysm as flow is relaxed because of the aneurysmal expansion. At t/T=0, maximum WSS for stenosis and aneurysm are 18 and 2.6 respectively. At t/T=0.25, when the flow quickly accelerates, the maximum WSS for stenosis and aneurysm becomes 37 and 3 respectively. At t/T=0.50, the maximum WSS for stenosis and aneurysm becomes 16 and 1.0 respectively. At t/T=0.75, maximum WSS for stenosis and aneurysm are 2 and 0.5 respectively. Out of all times the maximum WSS is found when the flow accelerates at t/T=0.25. In all the cases, the maximum WSS developed in the stasis is much higher than that developed in aneurysm.

3.4 WSS Comparison between 48% stenosis and 48% aneurysm

3.4.1 WSS at Wo=7.75

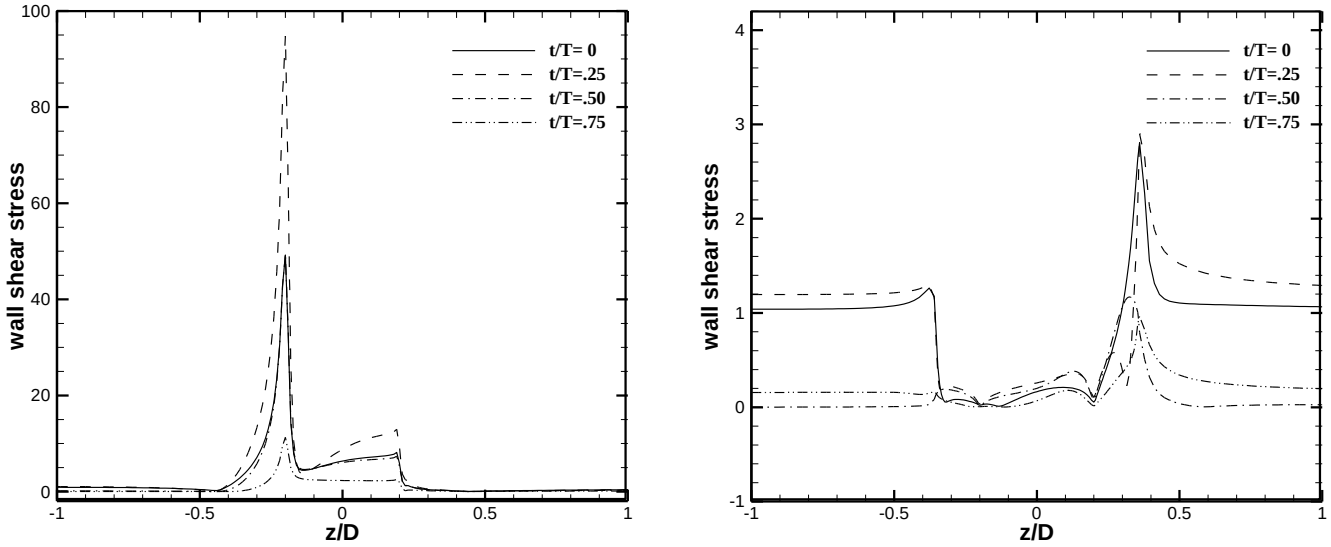

Figure 33: WSS distribution at four key flow time for (a)stenosis and (b) aneurysm

Here, in the figure 33, for the 32% stenosis/aneurysm with a flow having Wo=10, the Wall Shear Stress distributions along the axial direction in the wall for different times are presented. It is clearly observed that for the stenosis, the WSS is highest at the inlets sections of the stenosis as the flow is hitting directly to the inlet side of the stenosis causing the abrupt increase of WSS, a bit higher throughout the stenosis area and finally drops down after the outlet sections. But for the aneurysm, the WSS behavior is different from that of stenosis. Here, the maximum WSS is found at the outlet sections of the aneurysm as the flow expanding form the inlet sides hits the outlet side creating high WSS. For the times when the fluid accelerates, the WSS maintains a bit higher value throughout the axial length and finally abruptly reduces and becomes minimum inside the aneurysm as flow is relaxed because of the aneurysmal expansion. At t/T=0, maximum WSS for stenosis and aneurysm are 18 and 2.6 respectively. At t/T=0.25, when the flow quickly accelerates, the maximum WSS for stenosis and aneurysm becomes 37 and 3 respectively. At t/T=0.50, the maximum WSS for stenosis and aneurysm becomes 16 and 1.0 respectively. At t/T=0.75, maximum WSS for stenosis and aneurysm are 2 and 0.5 respectively. Out of all times the maximum WSS is found when the flow accelerates at t/T=0.25. In all the cases, the maximum WSS developed in the stasis is much higher than that developed in aneurysm.

3.4.2 WSS at Wo=10

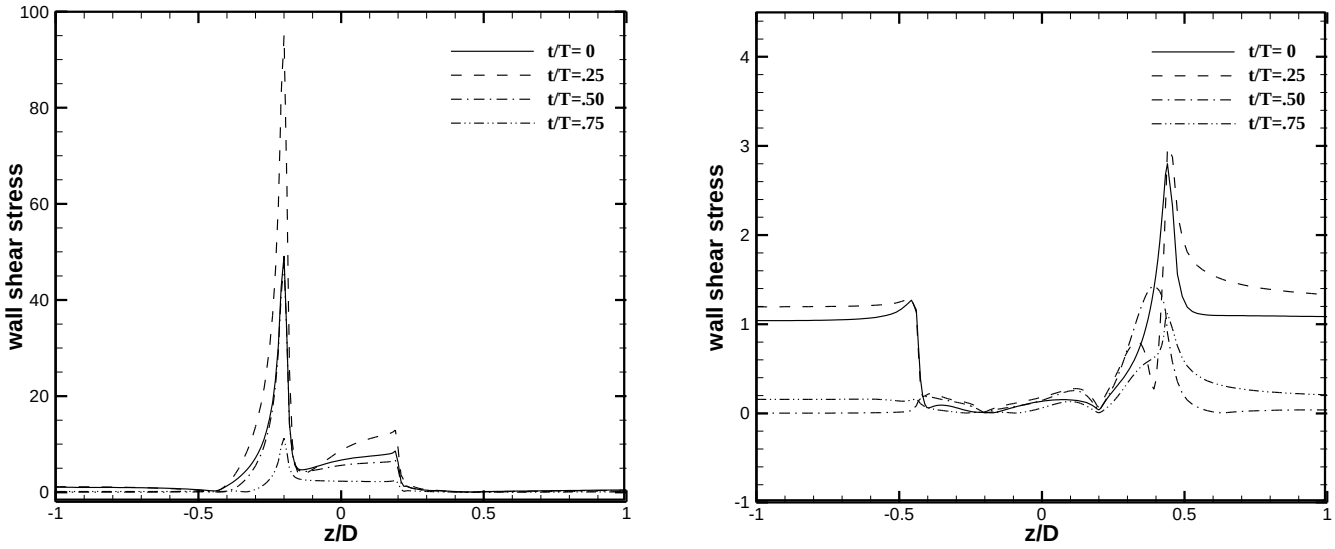

Figure 34: WSS distribution at four key flow time for (a)stenosis and (b) aneurysm

Here, in the figure 34, for the 48% stenosis/aneurysm with a flow having Wo=10, the Wall Shear Stress distributions along the axial direction in the wall for different times are presented. It is clearly observed that for the stenosis, the WSS is highest at the inlet sections of the stenosis as the flow is hitting directly to the inlet side of the stenosis causing the abrupt increase of WSS, a bit higher throughout the stenosis area and finally drops down after the outlet sections. But for the aneurysm, the WSS behavior is different from that of stenosis. Here, the maximum WSS is found at the outlet sections of the aneurysm as the flow expanding form the inlet sides hits the outlet side creating high WSS. For the times when the fluid accelerates, the WSS maintains a bit higher value throughout the axial length and finally abruptly reduces and becomes minimum inside the aneurysm as flow is relaxed because of the aneurysmal expansion. At t/T=0, maximum WSS for stenosis and aneurysm are 50 and 2.8 respectively. At t/T=0.25, when the flow quickly accelerates, the maximum WSS for stenosis and aneurysm becomes 97 and 3.2

respectively. At t/T=0.50, the maximum WSS for stenosis and aneurysm becomes 11 and 1.2 respectively. At t/T=0.75, maximum WSS for stenosis and aneurysm are 10 and 0.5 respectively.Out of all times the maximum WSS is found when the flow accelerates at t/T=0.25. In all the cases, the maximum WSS developed in the stasis is much higher than that developed in aneurysm.

3.5 Effect of Womersley Number

To evaluate the effects of Womersley number, the details of the velocity distribution and the change of the WSS for two different Womersley numbers were taken having the same Reynolds number. Effects were observed for different depths of stenosis and aneurysm. The Womersley numbers taken were 7.75 and 10 for a constant mean Reynolds number of 578 with a highest and lowest number of 928 and 228.

Womersley number is found to have a little effect in the velocity distribution both in the case of the stenosis and aneurysm for the particular models of stenosis and aneurysm used. The velocity magnitudes are not affected significantly because of this change of the Womersley number from 7.75 to 10.

Because of the very little effect of Womersley number on the velocity distribution, it has too the same little effect on the WSS found both in the aneurysm and stenosis. Both 32% and 48% stenosis and aneurysm were observed and they have shown almost same type of effect.

Womersley number is the physical interpretation of the effect of the unsteadiness to the viscous effect of the flow. Dynamic nature of the flow is greatly dependent on the flow frequency of the

flow. For the two frequencies of time periods 345 milliseconds and 200 milliseconds it has been observed that viscous force is dominant in the flow of the chosen models of stenosis and aneurysm.

3.6 Effect of Size/Severity of stenosis and aneurysm

Table 02: presentation of flow parameters at different severities of stenosis and stenosis

Size/ Severity	model	Centerline velocity at t/T=0.25 (# of times of mean velocity)			WSS (Pa)
		Just Inlet	Throat	Just Outlet	
32%	stenosis	3.18	4.2	4.3	35
	aneurysm	2.6	2.5	2.6	2.5
48%	stenosis	3.5	6.95	7.1	95
	aneurysm	2.6	2.42	2.58	3

It can be said with certainty that size or the severity has great effect on the flow field of the constricted tubes of stenosis and less effect on aneurysm for the models considered. For investigating the effect of stenosis size/aneurysm size, different stenosis and aneurysm models with two different sizes have been studied. In the Just Inlet section, at t/T=.25 when the flow is accelerating, for the constant flow frequency, the centerline velocities of the stenosis and aneurysm are 3.18 and 2.6 times of the mean velocity for the 32% severity. Whereas, for 48% severity, centerline velocities are 3.5 times and 2.6 times of the mean velocities showing a large variation in the stenosis and insignificant variation of velocities in the aneurysm for the given models of stenosis and aneurysm. In the Throat, at t/T=.25 when the flow is accelerating, for the constant flow frequency, the centerline velocities of the stenosis and aneurysm are 4.2 and 2.5 times of the mean velocity for the 32% severity. Whereas, for 48% severity, centerline velocities

are 6.95 times and 2.42 times of the mean velocities showing a large variation in the stenosis and small variation of velocities in the aneurysm for the given models of stenosis and aneurysm. When the depth of the stenosis is increased the flow area for the stenosis decreases and as such the velocity will increase but with the increase of the severity of the aneurysm the flow area increases. Though the flow is dependent on the total flow pattern inside the aneurysmal sac, the velocity is likely to decrease because of the increase of area.

As the size/severity has great effect on the velocity distribution of the stenosis and aneurysm, it will have great influence on the WSS distribution on the walls of the stenosis and aneurysm. WSS developed is maximum when the flow is accelerating that is at t/T=0.25. Maximum shear stresses developed in stenosis and aneurysm for the severity of 32% are 35 and 2.5 respectively. Whereas for 48% severity, the WSS becomes 95 and 3 respectively indicating 170% and 20% increase for stenosis and aneurysm respectively. They are measured for the same flow frequency.

In the aneurysm it has been seen that the radial velocity at the throat has decreased when the severity is increased while there is an increase in the WSS. In the middle of the increase of the area there is decrease of velocity but inside the sac of the aneurysm, because of the creation of turbulence, there is increase of the Wall Shear Stress.

For the particular models chosen for stenosis and aneurysm, it has been observed that the size/severity has great effect on the flow field and WSS. And the effects are much greater in stenosis than in aneurysm

4 Conclusions

In the present study, a numerical simulation has been presented to investigate the effects of laminar sinusoidal flow through the modeled arterial stenosis and aneurysm. For both the models, the trapezoidal profile with an angle of 45^0 has been used to observe the effects on them. The models were axisymmetric. Sizes were varied from 32% severity to 48% severity with the corresponding depth of 1.6mm and 2.4mm respectively. Inlet flow given was the sinusoidal pulsating with a mean Reynolds Number of 578 having maximum of 928 and a minimum value of 228.Womersley numbers of 7.75 and 10 with a time periods of 345 milliseconds and 200 milliseconds respectively were used to see the effect of the change of the flow pulsation. Radial velocity distribution and Wall Shear Stress distribution have been observed to see the effects of change of Womersley number and sizes of the stenosis and aneurysm.

From the numerical simulation, the following conclusions can be drawn-

1. Variation of Womersley number is found to have a little effect in the velocity distribution both in the case of the stenosis and aneurysm for the particular models of stenosis and aneurysm used. This implies that the viscous force is dominant on the flow.
2. As Viscous force is dominant on the flow, Womersley number has little effect on the WSS found both in the aneurysm and stenosis. Both 32% and 48% stenosis and aneurysm were observed and they have shown almost same type of effect.
3. It can be stated with certainty that size or the severity of the stenosis has great effect on the flow field of stenosis while the severity shows a little effect for aneurysm for the particular models considered. In the Throat, at t/T=.25 when the flow is accelerating, for the constant flow frequency, the centerline velocity of the stenosis for 48% severity is

1.65 times of that of 32% severity. Whereas, the centerline velocity of the aneurysm for 48% severity is .97 times of that of 32% severity.

4. As the size/severity has great effect on the velocity distribution of the stenosis, it will have great influence on the WSS distribution on the walls of the stenosis. WSS developed is maximum when the flow is accelerating that is at t/T=0.25. Maximum shear stresses developed in stenosis and aneurysm of 48% shows 170% and 20% increase than that of 32% stenosis respectively.
5. For a particular depth of stenosis and aneurysm, with the same flow inputs, WSS is too high in the stenosis compared to that in aneurysm indicating very high risk in stenosis.
6. It has been observed that, for the stenosis, the WSS is highest at the inlet sections of the stenosis as the flow is hitting directly to the inlet side of the stenosis causing the abrupt increase of WSS. But for the aneurysm, the WSS behavior is different from that of stenosis. Here, the maximum WSS is found at the outlet sections of the aneurysm as the flow expanding form the inlet sides hits the outlet side creating high WSS.

5 Bibliography

1. Staff, M.A., *Top 10 Most Important Human Body Organs.* 2017.
2. Institute, H.V., *Anatomy and Function of the Heart Valves.* 2018.
3. Hyperion., *Amazing Heart Facts.* 2000.
4. R., S., *Which chamber of the heart receives deoxygenated blood from the body?* 2016.
5. Md. Iqbal Hossain, N.S., *Simulation of Mass Transfer Phenomenon in a CAD Drug Eluting Stent* 2017.
6. Barry M O'Connell, T.M.M., *Factors that affect mass transport from drug eluting stents into the artery wall.* Biomed Eng Online, 2010.
7. D'Souza, D.D., *Blood vessel wall composition.* 2009.
8. Institute, N.H., *Coronary Heart Disease.*
9. Institute, N.H., *Coronary Artery Bypass Grafting.*
10. Institute, A.H., *What is Heart Failure?* 2017.
11. Julien, D.W., *Peripheral Arterial Disease.* 2016.
12. *Causes of death.* 15th Greek Australian Legal and Medical Conference Thessaloniki, Greece 2015, 2015.
13. Channel, B.H., *Aneurysm.* 2013.
14. Clinic, M., *Thoracic aortic aneurysm.* 2018.
15. Doyle, B.J., et al., *Identification of rupture locations in patient-specific abdominal aortic aneurysms using experimental and computational techniques.* Journal of biomechanics, 2010. **43**(7): p. 1408-1416.
16. Holly Kerr, A., *Aortic Aneurysms.*
17. Berger, S. and L.-D. Jou, *Flows in stenotic vessels.* Annual Review of Fluid Mechanics, 2000. **32**(1): p. 347-382.
18. Buchanan, J.R., et al., *Relation between non-uniform hemodynamics and sites of altered permeability and lesion growth at the rabbit aorto-celiac junction.* Atherosclerosis, 1999. **143**(1): p. 27-40.
19. Ojha, M., et al., *Pulsatile flow through constricted tubes: an experimental investigation using photochromic tracer methods.* Journal of fluid mechanics, 1989. **203**: p. 173-197.
20. Mittal, R., S. Simmons, and H. Udaykumar, *Application of large-eddy simulation to the study of pulsatile flow in a modeled arterial stenosis.* Journal of biomechanical engineering, 2001. **123**(4): p. 325-332.
21. Niazmand, H., A. Sepehr, and P. Shahabi. *Numerical analysis of aneurysm using pulsatile blood flow through a locally expanded vessel*. in *ECCOMAS CFD 2006: Proceedings of the European Conference on Computational Fluid Dynamics, Egmond aan Zee, The Netherlands, September 5-8, 2006*. 2006. Delft University of Technology; European Community on Computational Methods in Applied Sciences (ECCOMAS).
22. TOUFIQUE, H.A. and D.K. Das, *Numerical simulation of sinusoidal fluctuated pulsatile laminar flow through stenotic artery.* 2008.
23. Ali, N., A. Zaman, and M. Sajid, *Unsteady blood flow through a tapered stenotic artery using Sisko model.* Computers & Fluids, 2014. **101**: p. 42-49.
24. Chan, W., Y. Ding, and J. Tu, *Modeling of non-Newtonian blood flow through a stenosed artery incorporating fluid-structure interaction.* Anziam Journal, 2007. **47**: p. 507-523.

25. Ahmed, S.A. and D.P. Giddens, *Pulsatile poststenotic flow studies with laser Doppler anemometry.* Journal of biomechanics, 1984. **17**(9): p. 695-705.
26. Deshpande, M., D. Giddens, and R. Mabon, *Steady laminar flow through modelled vascular stenoses.* Journal of Biomechanics, 1976. **9**(4): p. 165-174.
27. Huang, H., V. Modi, and B. Seymour, *Fluid mechanics of stenosed arteries.* International Journal of Engineering Science, 1995. **33**(6): p. 815-828.
28. Ishikawa, T., et al., *Effect of non-Newtonian property of blood on flow through a stenosed tube.* Fluid dynamics research, 1998. **22**(5): p. 251-264.
29. Lee, T., *Numerical studies of fluid flow through tubes with double constrictions.* International journal for Numerical methods in Fluids, 1990. **11**(8): p. 1113-1126.
30. Liao, W., T. Lee, and H. Low, *Numerical study of physiological turbulent flows through stenosed arteries.* International Journal of Modern Physics C, 2003. **14**(05): p. 635-659.
31. Mahapatra, T.R., G. Layek, and M. Maiti, *Unsteady laminar separated flow through constricted channel.* International journal of non-linear mechanics, 2002. **37**(2): p. 171-186.
32. Neofytou, P. and S. Tsangaris, *Flow effects of blood constitutive equations in 3D models of vascular anomalies.* International journal for numerical methods in fluids, 2006. **51**(5): p. 489-510.
33. Tu, C. and M. Deville, *Pulsatile flow of non-Newtonian fluids through arterial stenoses.* Journal of biomechanics, 1996. **29**(7): p. 899-908.
34. Zendehbudi, G. and M. Moayeri, *Comparison of physiological and simple pulsatile flows through stenosed arteries.* Journal of Biomechanics, 1999. **32**(9): p. 959-965.
35. Kumar, B.R. and K. Naidu, *Finite element analysis of nonlinear pulsatile suspension flow dynamics in blood vessels with aneurysm.* Computers in biology and medicine, 1995. **25**(1): p. 1-20.
36. Husain, I., C. Langdon, and J. Schwark, *Non-Newtonian pulsatile blood flow in a modeled artery with a stenosis and an aneurysm.* Rec. Res. Envi. Geo. Sc: p. 413-418.
37. Gopalakrishnan, S.S., B. Pier, and A. Biesheuvel, *Dynamics of pulsatile flow through model abdominal aortic aneurysms.* Journal of Fluid Mechanics, 2014. **758**: p. 150-179.
38. Finol, E., K. Keyhani, and C. Amon, *The effect of asymmetry in abdominal aortic aneurysms under physiologically realistic pulsatile flow conditions.* Journal of biomechanical engineering, 2003. **125**(2): p. 207-217.

Appendix

Table: Literature on stenosis and aneurysm

SL No.	**author**	**Method/model/ type of study**	**Finding**
01	Ojha et al.	Photochromic tracer method	➢ With mild constrictions of the stenosis, isolated regions of vortical and helical structures were observed ➢ For moderate constrictions of stenosis, transition to turbulence was triggered just before peak flow through the breakdown of waves and streamwise vortices ➢ During this vortex generation phase of the flow cycle, the wall shear stress fluctuated quite intensely
02	Mittal et al.	The technique of large-eddy simulation (LES)	➢ At a Reynolds number of 2000, the flow downstream of the stenosis transitions to turbulence and exhibits all the classic features of post-stenotic flow which include the periodic shedding of shear layer vortices and transition to turbulence downstream of the stenosis.
03	Modarres et al.	Rheology models (Newtonian, Power law and Quemada)	➢ Quemada model always located between Newtonian and Power law models however its behavior is closer toPower law model ➢ Quemada results are more realistic and accurate.
04	Toufique et al.	Numerical Study	➢ The dynamic nature of pulsating flow disturbs the radial velocity distribution and thus generates recirculation zone in the post stenotic region. ➢ Peak wall shear stress and wall vorticity appear to intense at the throat of the stenosis ➢ The peak wall vorticity seems to increase with the increase of stenosis size and Reynolds number

05	W. Y. Chan et al.	Numerical simulation using Newtonian, Power Law and the Carreau non Newtonian models	➢ When compared to the Newtonian flow models, the result from the Carreau model showed very little difference, in terms of velocity, pressure and wall shear stress, whereas the result from the Power Law model showed more significant vortices and smaller wall shear stresses. ➢ The highest stress concentration was also found at the throat of the stenosis.
06	Ahmed et al.	laser Doppler anemometry	➢ A permanent region of poststenotic flow separation does not exist even for the severest constriction, in contrast to results for steady flow. ➢ Values of wall shear stress were greatest near the throat of the constriction and were relatively low in the poststenotic region ➢ identification of flow disturbances of an organized nature may be fundamental in recognizing mild to moderate disease
07	Deshpande et al.	numerical solutions	➢ No difficulties in convergence are encountered for Reynolds numbers at which the flow is known to be laminar from experimental observation
08	Huang et al.	finite difference scheme	➢ There is a correlation between regions of recirculation, which are a prominent feature of the unsteady flow, and the location of lesions ➢ Experimental measurements for steady flow complement the numerical study and show qualitative agreement.

09	Ishikawa et al.	numerically analysis	➢ Non-Newtonian property reduces the strength of the vortex downstream of stenosis and has considerable influence on the flow even at high Stokes and Reynolds numbers, provided that pulsatile flow has a stagnant period.
10	Lee et al.	Numerically study	➢ the peak value of wall vorticity is found slightly upstream of each of the constrictions of stenosis ➢ When the Reynolds number is increased, the peak wall vorticity value increases and its location is moved upstream ➢ Maximum wall vorticity generated by the first constriction is found to be always greater than the maximum wall vorticity generated by the second constriction
11	Liao et al.	Numerically study	➢ The larger Reynolds number and severer constriction ratio may result in more complex flow field and cause some important flow variables to increase dramatically near stenosis. ➢ The higher Womersley number leads to a larger phase lag between the imposed flow rate changes and the final converged flow field in one cycle ➢ The turbulence intensity decreases with the increase of Womersley number for the same Reynolds number.

12	Mahapatra et al.	Numerically study	➢ The critical Reynolds number for asymmetric flow through a symmetric constriction has been found ➢ Critical values depend on the area reduction and the length of the constriction. ➢ An increase of Reynolds number grows the asymmetry of the flow. ➢ For flow through symmetric constriction the centerline vertical velocity exhibits finite oscillation behind the constriction at high Reynolds number.
13	Neofytou et al.	Numerically study	➢ Results show marked differences between simulating blood as Newtonian and non-Newtonian fluid and furthermore the Power-Law model exhibits different behaviour in all cases compared to the other models whereas Quemada and Casson models exhibit similar behavior in the case of the stenosis but different behavior in the case of the aneurysm.
14	Tu et al.	Newtonian model	➢ The memory effects taken into account in the model affect deeply the flow compared with the Newtonian reference case. ➢ The disturbances are stronger by their vorticity intensity and persist after the geometrical obstacle.
15	Zendehbudi and Moayeri	Numerical study	➢ for thorough understanding of pulsatile flow behavior in stenosed arteries, the actual physiological flow should be simulated

16	Kumar et al.	transient UVP finite element method (FEM)	➢ The central axis velocity, central axis and wall pressures, pressure gradient history, and wall shear stress are influenced by the presence of aneurysm. ➢ Time-dependent recirculation regions which are sensitive to the degree of dilation of the vessel are seen in the concavity of the dilation ➢ High shear stresses were noticed near the ends of aneurysm that can lead to the development of stenosis in the region downstream from the dilation of the vessel.
17	Husain et al.	Numerical study	➢ There are significant differences between simulating blood as a Newtonian or non- Newtonian fluid. ➢ Newtonian model is a good approximation in regions of mid-range to high shear but the Generalized Power Law model provides a better approximation of wall shear stress at low shear.
18	Gopalakrishnan et al.	Numerical study	➢ The abdominal aortic aneurysm can be viewed as acting like a 'wavemaker' that induces disturbed flow conditions in healthy segments of the arterial system far downstream of the aneurysm ➢ a sensitivity analysis is appropriate when a patient-specific computational study is carried out to obtain a quantitative description of the wall shear stress distribution.
19	Finol et al	Numerical study	➢ Peak wall shear stress and peak wall pressure are reported as a function of the time-average Reynolds number and aneurysm asymmetry ➢ The effect of asymmetry in hypothetically shaped AAAs is to increase the maximum wall shear stress at peak flow and to induce the appearance of secondary flows in late diastole.